GPM Combined Radar-Radiometer Precipitation Algorithm Theoretical Basis Document (Version 5)

William S. Olson

and the

GPM Combined Radar-Radiometer Algorithm Team

January 8, 2018

Table of Contents

1. Introduction

The GPM Combined Radar-Radiometer Algorithm performs two basic functions: first, it provides, in principle, the most accurate, high resolution estimates of surface rainfall rate and precipitation vertical distributions that can be achieved from a spaceborne platform, and it is therefore valuable for applications where information regarding instantaneous storm structure are vital. Second, a global, representative collection of combined algorithm estimates will yield a single common reference dataset that can be used to "cross-calibrate" rain rate estimates from all of the passive microwave radiometers in the GPM constellation. The cross-calibration of radiometer estimates is crucial for developing a consistent, high time-resolution precipitation record for climate science and prediction model validation applications. Because of the Combined Algorithm's essential roles as accurate reference and calibrator, the GPM Project is supporting a Combined Algorithm Team to implement and test the algorithm prior to launch. In the pre-launch phase, GPM-funded science investigations led to significant improvements in algorithm function, and the basic algorithm architecture was formulated. This algorithm architecture is largely consistent with the successful TRMM Combined Algorithm design, but it has been updated and modularized to take advantage of improvements in the representation of physics, new climatological background information, and model-based analyses that may become available at any stage of the mission. Post-launch, algorithm physical parameterizations for effects such as the non-uniform beamfilling of the radar footprint by rain and multiple scattering of radar pulses by ice-phase precipitation have been improved. Also, the radiative effects of nonspherical ice-phase precipitation and a semi-emprical model relating radar surface backscatter cross-section and multi-spectral microwave emissivities have been included. This document presents a description of the GPM Combined Algorithm architecture, scientific basis, supporting ancillary datasets, inputs/outputs, and testing plan.

2. Background

GPM Instruments

The GPM core mission satellite observatory is shown in Fig. 1. From this platform, the Dual-frequency Precipitation Radar (DPR) scans cross-track in relatively narrow swaths at Ku band (13.6 GHz) and Ka band (35.5 GHz). The dual-frequency radar reflectivity observations are nearly beam-matched over the 125 km Ka-band swath, with a horizontal resolution of approximately 5 km, and a vertical resolution of 250 m in standard observing mode. The Ku band radar scans over a wider, 245 km swath. The GPM Microwave Imager (GMI) scans conically over an 885 km wide swath at frequencies of 10.65, 18.7, 23.8, 36.5, 89.0, 165.5, 183.31 ± 7, and 183.31 ± 3 GHz. Measured brightness temperatures are in two polarizations (vertical and horizontal) at all but the 23.8 GHz and 183.3 GHz channels, which provide only vertical polarization

measurements. The GMI observations are diffraction limited, with the lowest-resolution footprints (approx. 26 km) at 10.7 GHz and the highest-resolution footprints (approx. 6 km) at the 89.0 GHz and higher frequency channels.

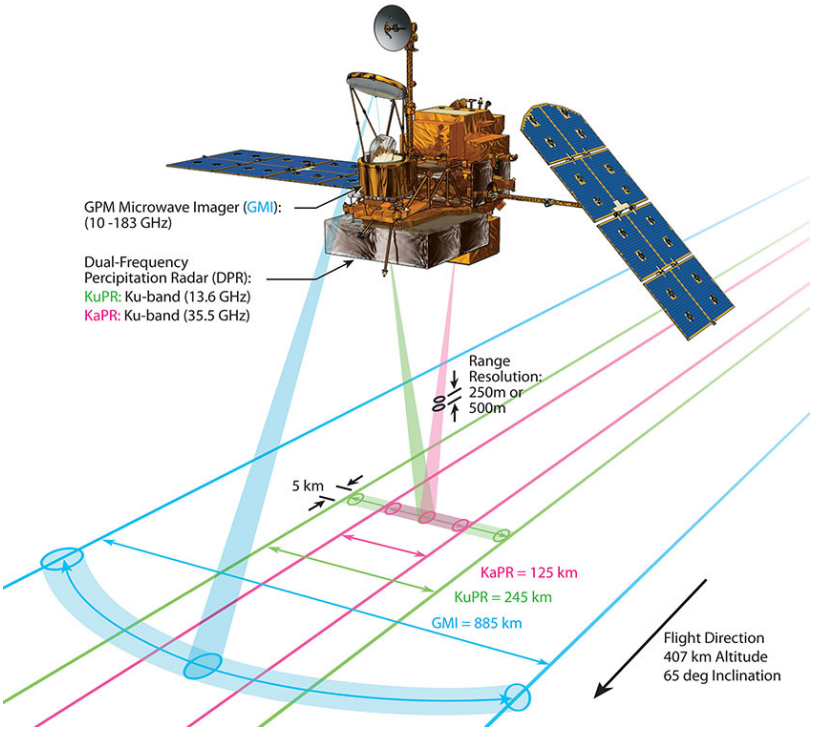

Fig. 1. Configuration of the GPM core observatory, illustrating the scanning geometry of the DPR and GMI instruments.

Implications for Algorithm Design

The current GPM Combined Radar-Radiometer Algorithm architecture is descended from a rich heritage of algorithms that were developed for the TRMM mission, as well as other algorithms developed and applied to airborne radar-radiometer data. In TRMM, only Ku-band radar observations were available from the radar instrument (the Precipitation Radar, or PR), and only lower-frequency (10 - 85 GHz) brightness temperature measurements were available from the microwave radiometer (the TRMM Microwave Imager, or TMI). The TRMM Facility Combined Algorithm used radiometer information to essentially reduce uncertainties in estimates of radar-derived total path-integrated attenuation to the earth's surface to perform an improved attenuation correction of the radar reflectivity vertical profile. The improved attenuation correction was effected by adjusting a single parameter of the precipitation particle-size distribution over the entire precipitation vertical profile. This single parameter represented a rain-normalized, mass-weighted mean particle diameter, which was assumed to be locally constant over the scale of TMI footprints. Adding horizontal variations of this parameter would have introduced too many free parameters to the inversion problem.

The GPM Combined Algorithm takes advantage of the additional Ka band

radar channel to glean more specific information about the precipitation size distribution and associated attenuation in each gate. The estimation of precipitation size distribution parameters is further aided by precipitation attenuation information from the GMI channels, which have an extended spectral range relative to the TMI. However, if the Ka band reflectivities do not provide additional information due to very light rain (Rayleigh limit), or they are severely attenuated in heavy precipitation, then the combined algorithm must make a natural transition to a single-frequency, Ku band solution in which a more approximate estimation of precipitation size distribution parameters is performed.

Regardless of whether or not the Ka band data are applicable, however, information from the GMI brightness temperatures can be used to make further adjustments of path attenuation due to non-precipitating cloud liquid water and water vapor, which are not directly sensed by the DPR. In addition, there are precipitation microphysical parameters, such as the intercept of the particle size distribution and the density of ice-phase precipitation that may be adjusted using radiometer information.

Ultimately, the degree to which any precipitation or environmental parameters can be adjusted is limited by the information content of the DPR and GMI observations and any additional information provided by *a priori* data, such as the natural ranges of particle size distribution parameters, cloud water contents, etc., and how these parameters covary spatially. Therefore, as outlined in section 3, the combined algorithm is designed to be able to accept both different physical modeling assumptions and *a priori* constraints on estimated parameters.

3. Algorithm Architecture

Overview

The current algorithm design is based upon an Ensemble Filtering (EnF) approach for inverting the DPR reflectivities and GMI brightness temperatures to estimate precipitation profiles; see Anderson (2003) for a general description of EnF approaches. The general architecture of the GPM Combined Algorithm is illustrated in Fig. 2a,b. There are four primary modules in the Combined Algorithm: the Ku Radar Module, which produces ensembles of Ku radar-consistent precipitation profile solutions at each DPR footprint location, the Forward Model Module, that simulates the remaining DPR and GMI measurements, the Radiance Enhancement Module, which estimates what the GMI brightness temperatures would be at the resolution of the DPR, and the Filter Module, that modifies the Ku radar-derived precipitation ensembles to be more consistent with remaining observations. The outputs of the algorithm are the mean (best estimate) and standard deviation (uncertainty of estimate) of the DPR-GMI filtered ensemble of estimated precipitation profiles at each DPR

footprint location. Following is a description of algorithm flow from the ingest of satellite sensor data to the output of precipitation estimates.

The Combined Radar-Radiometer Algorithm first ingests Radar Algorithm Level 2 calibrated reflectivities at Ku and Ka bands (if available) as well as Level 1C intercalibrated brightness temperatures from the GMI. To stay within computer memory limitations, a maximum of 300 scan lines of DPR data and corresponding GMI data are processed by the algorithm at a time. Therefore, the flow diagram of Fig. 2a represents the processing of one swath segment, which is repeated until the entire orbit is processed. The DPR footprint locations define an

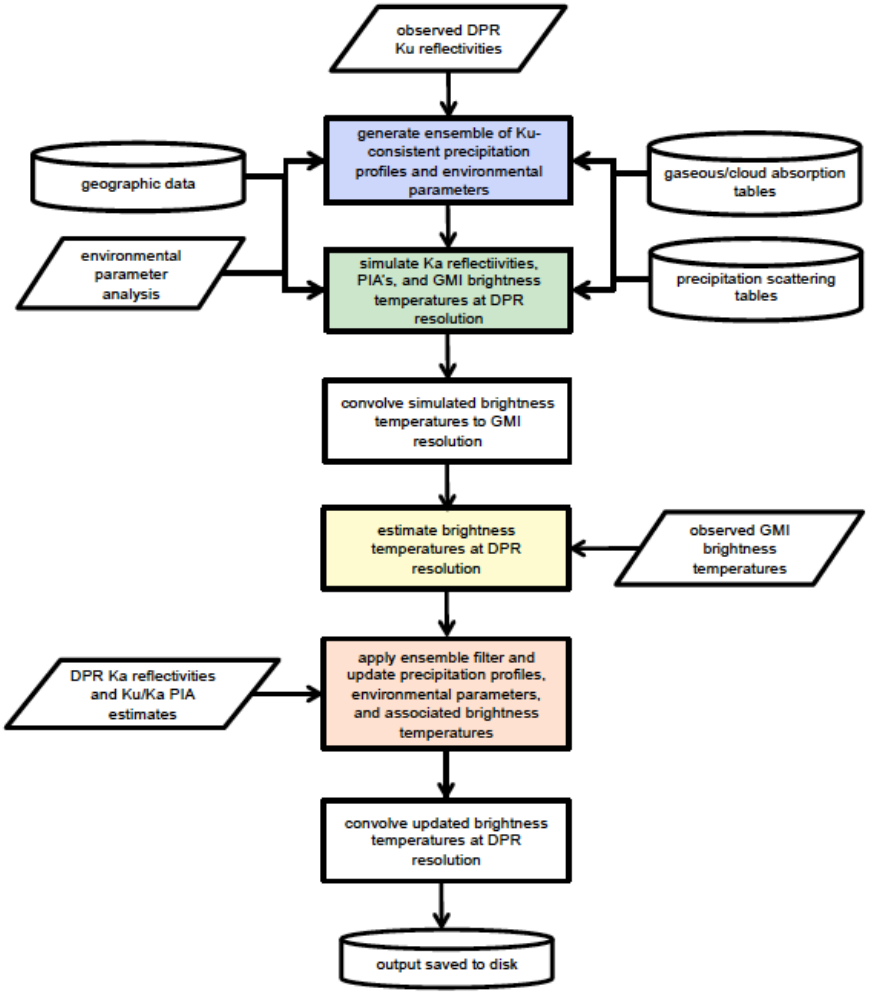

Fig. 2a. Processing schematic for the Combined Radar-Radiometer Algorithm. Ku Radar Module is in blue (see also Fig. 2b), Forward Model Module is in green, Radiance Enhancement Module is in yellow, and Filter Module is in orange.

approximate 5 km x 5 km grid on the earth's surface, and these footprints are used to represent the solution grid for algorithm-estimated precipitation profiles.

The first major process in the algorithm is the estimation of precipitation profiles in the Ku Radar Module. The first step in this process is to determine whether precipitation is detected in the column. The Ku Radar has a minimum detectable signal of approximately 13 dBZ, and range gates with reflectivities higher than this threshold at altitudes above the surface clutter are interpreted as precipitating. Precipitation detection and surface clutter information is provided by the Radar Algorithm Level 2 output.

If precipitation is detected, then the near-vertical column of Ku reflectivities is processed further to make initial estimates of precipitation. The precipitation estimation requires additional inferences of the pressure/temperature profile of the atmospheric column, the gaseous and cloud water absorption properties of the column, and whether or not the precipitation is convective or non-convective. The pressure/temperature is drawn from meteorological analysis data that have been interpolated to the locations of the Ku range bins, and these temperatures are provided by the Radar Algorithm Level 2 output. If a bright band of high Ku reflectivity is detected in the column, then this establishes a reference point in the phase-transition from ice to liquid in the column, with the transition starting 750 m above this point and ending 500 m below the point. Alternatively, if no bright band is detected, then the freezing level in the analysis temperature profile provides the reference point.

Gaseous absorption depends on the pressure, temperature, and humidity of the atmosphere. Cloud absorption depends on the temperature and cloud water content. Since the water vapor and cloud water distributions are not well known *a priori*, and since first guess estimates of water vapor and cloud cannot be reliably determined from global analyses, prospective water vapor and cloud profiles are generated from EOF representations derived from cloud-system-resolving model simulations. Random weightings of the EOF components are used to generate ensembles of possible water vapor and cloud vertical profiles that could occur, *a priori*. An ensemble of 40 profiles is created in this way.

Along with the *a priori* ensembles of water vapor and cloud profiles, *a priori* assumptions regarding the precipitation particle size distribution at each range bin are also made. The precipitation particle size distribution (PSD) in each bin is described by a normalized gamma distribution (Testud et al. 2001),

$$n(D) = N_w f(\mu) \left(\frac{D}{D_m} \right)^{\mu} \exp\left(-\frac{(4+\mu)}{D_m} D \right), \quad (1)$$

where

$$f(\mu) = \frac{6(4+\mu)^{\mu+4}}{4^4 \Gamma(4+\mu)}. \quad (2)$$

Here, N_w is the intercept of the normalized distribution, D_m is the volume-

weighted mean diameter, μ is the distribution shape factor, D is the liquid-water equivalent diameter of the particle, and $n(D)$ is the spectral number density of particles with diameter D.

Since there are three parameters that describe the precipitation PSD and at most two independent radar-derived reflectivity observations associated with each DPR range bin, assumptions regarding the PSD parameters are made to reduce the degrees of freedom in the estimation problem. In the current algorithm, μ is assumed constant, and it is currently set at a value of 2. Ensembles of prospective N_w profiles are generated using an autoregressive function, starting with a random value drawn from an assumed pdf at the top of the profile. The assumed pdf depends on the convective vs. non-convective classification of the given profile; this classification is output from the Radar Algorithm Level 2, and it is based upon the horizontal and vertical structures of Ku reflectivity in the DPR observations. Each ensemble member N_w profile and constant μ profile is matched to a water vapor and cloud profile from the ensemble of water vapor and cloud profiles. This creates a combined *a priori* ensemble of environmental and precipitation parameter profiles, and only the third PSD parameter, D_m, is not specified in each ensemble profile. The third parameter, D_m, in each range bin is inverted from the profile of Ku band reflectivities for each ensemble member profile, as described forthwith.

To estimate D_m for each ensemble member profile, the reflectivity profile at Ku band is first corrected for gaseous and cloud water attenuation in each of the 40 ensemble member environmental profiles. The specific absorption by atmospheric gases and cloud water as a function of pressure, temperature, humidity and cloud water content is drawn from tabulated values at the Ku band frequency. The remaining attenuation in each ensemble member reflectivity profile is due to precipitation.

Using the gas/cloud absorption-corrected Ku reflectivity profile, $\mathbf{Z_{Ku}}$, associated with a given ensemble member, a generalized Hitschfeld-Bordan method is applied to solve for the profile of D_m for that member; see Grecu et al. (2011). The generalized Hitschfeld-Bordan method is a single-wavelength, forward recursive method that iteratively computes the effective reflectivity and extinction by precipitation in a given range bin; then attenuation-corrects the reflectivity in the next range bin of the profile; see Fig. 2b. In the generalized approach, the iteration of reflectivity and extinction calculations is made computationally efficient through an analytical manipulation of the radar equation; see Grecu et al. (2011). The iteration equation is

$$Z(r) = \frac{Z_{Ku}(r)}{\left[1 - q\int_0^r Z_{Ku}^{\beta}(s)\,\frac{k(Z(s))}{Z^{\beta}(s)}\,ds\right]^{1/\beta}}, \qquad (3)$$

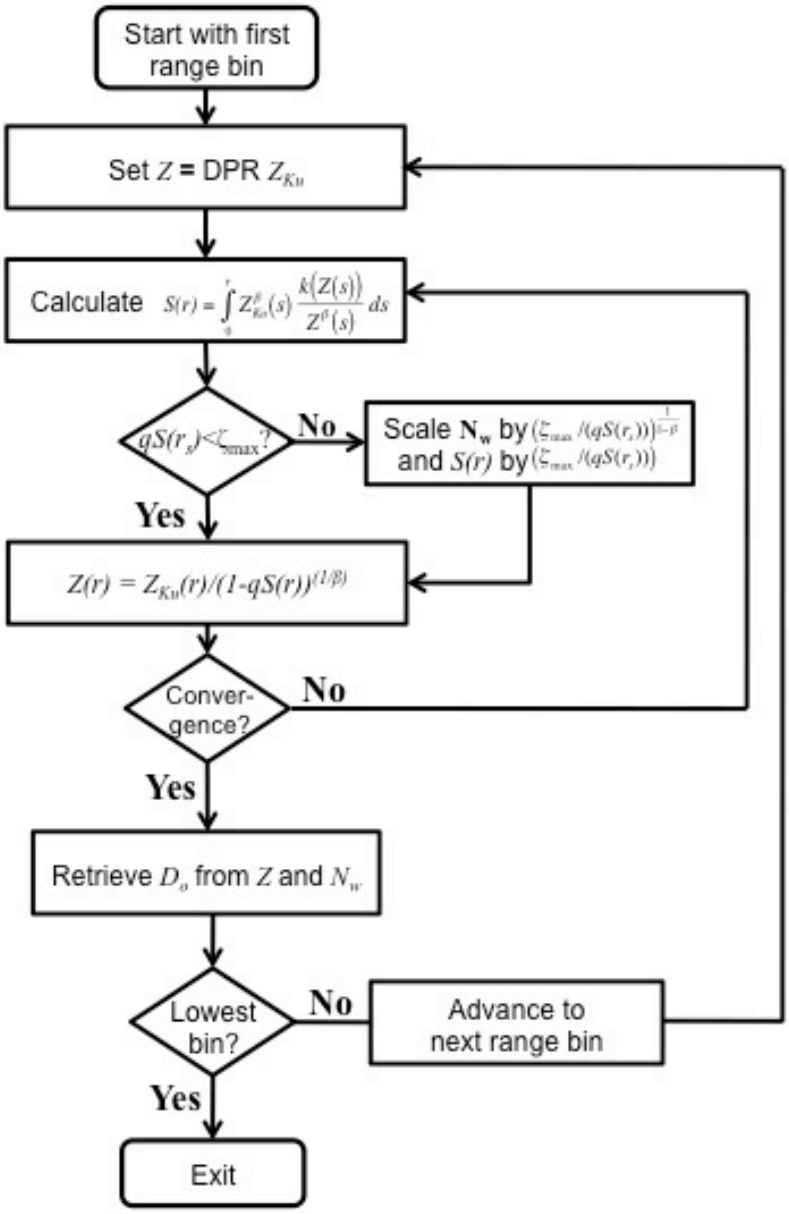

Fig. 2b. Schematic for the generalized Hitschfeld-Bordan method, contained in the Ku Radar Module; see Fig. 2a.

where $Z(r)$ is the attenuation-corrected reflectivity at range r, $Z_{Ku}(r)$ is the measured reflectivity at that range, $k(Z)$ is the specific extinction corresponding to reflectivity Z, $q = 0.2 \ln(10)$, and $k = \alpha Z^{\beta}$ is an approximate k-Z relation that is introduced to reduce the number of iteration steps. The actual relationships between precipitation extinction and reflectivity are represented by static "scattering" tables of these quantities for a range of N_w and D_m values, given μ. In high-attenuation regimes, numerical instabilities are avoided by rescaling the N_w profile; see Fig. 2b. The generalized Hitschfeld-Bordan method is applied to all of the member profiles in the ensemble at each Ku-band footprint location.

At light rain rates where independent estimates of the column path-integrated attenuation from the Level 2 Radar algorithm (see Meneghini et al. 2000) are unreliable, the initial guess N_w is updated from the initial guess D_m using an empirical formula. The updated N_w will have the observed anti-correlated relationship with D_m; see Thompson et al. (2015). The updated N_w is used as a new first guess N_w, and the algorithm proceeds normally.

If valid Ka-band data and/or GMI brightness temperature data are available, the algorithm passes to the Forward Model Module; see Fig. 2a. For each ensemble member profile passed from the Ku Radar Module, the single scattering properties at Ka-band and the GMI channel frequencies at each radar bin location are calculated using the gaseous/cloud absorption and precipitation scattering tables previously described. The single-scattering properties are used to simulate the Ka reflectivities, $\mathbf{Z_{Ka}}$, and PIA's at Ku and Ka bands, PIA_{Ku} and PIA_{Ka}, respectively, for each of the 40 ensemble member profiles.

Simulations of $\mathbf{Z_{Ka}}$ and PIA are subject to the effects of non-uniform beamfilling of precipitation within the radar footprint, as well as multiple scattering of radar pulse energy. Non-uniform beamfilling is accommodated by generating a set of "downscaled" reflectivity profiles from each observed Ku-band profile. Each downscaled profile is a simple, scaled version of the observed profile, where the scaling is a random, lognormally-distributed parameter, and the mean of the downscaled profiles is constrained to be equal to the observed profile. The scaling leads to a set of profiles that have vertical coherence, as seen in convective precipitation structures, but the profile-to-profile variation in the set represents the effects of horizontal variability within the radar footprint. For each ensemble member, the generalized Hitschfeld-Bordan method is applied to all the downscaled reflectivity profiles in the set, assuming the *a priori* environmental and PSD parameters associated with the ensemble member. The Ka reflectivities and PIA's are then simulated for each solution profile of the downscaled set, and then the mean precipitation parameter solution profile and the mean simulated Ka profile/PIA's of the set are computed. These mean, "upscaled" quantities are considered the precipitation parameter profile and simulated $\mathbf{Z_{Ka}}$, PIA_{Ku}, and PIA_{Ka} associated with the given ensemble member. The standard deviation of the lognormally-distributed scaling parameter can be adjusted to reflect the intrinsic horizontal variability of precipitation according

to the environmental state. Currently, only separate values of the standard deviation for over-ocean and over-land applications of the algorithm are prescribed.

Although the lognormally-distributed set of reflectivity profiles, just described, fairly well represents the effects on footprint non-uniform beamfilling, it was later determined that the path-integrated attenuation at Ka band, in particular, was being overestimated. Using off-line, high-resolution simulations of attenuation based upon ground-based radar fields, it was found that the Ka-band path-integrated attenuation in vertical columns over DPR-sized footprints, derived using a Hitschfeld-Bordan method as it is done in the CMB algorithm, significantly overestimates Ka band path integrate attenuation in convective regions where the footprints are partially filled with precipitation. However, the degree of partial filling can be roughly estimated using a 3x3 array of DPR footprints centered on the footprint of interest. A scaling parameter based on the 3x3 array is introduced to modify the Hitschfeld-Bordan derived path-integrated attenuation at Ka band to properly account for partial filling of the radar footprint by precipitation. At Ku band, the effects of partial footprint filling on path-integrated attenuation are much smaller and are neglected at present.

Multiple scattering of radar pulses is important in precipitation columns where bulk scattering by ice-phase precipitation is significant, as in the core regions of strong convection (Battaglia et al. 2015). The effects of multiple scattering of radar pulses at Ka band are evaluated using the 1-D time-dependent radiative transfer method of Hogan and Battaglia (2008). The ensemble-mean *a priori* conditions are used to estimate the precipitation profile from the original Ku-band observations. Then the Ka-band reflectivities are simulated using both a single-scattering assumption and the multiple-scattering method of Hogan and Battaglia (2008). If the single and multiple-scattering solutions differ by more than a small tolerance, then the Ka reflectivities are simulated for each ensemble member using the multiple-scattering method, utilizing the mean scattering properties of the downscaled set of Ku-band profile solutions as input. This approach limits the computationally-intensive multiple-scattering calculations to situations where such calculations are needed.

To simulate the GMI brightness temperatures (at DPR resolution), the surface temperature and microwave emissivities must be specified for each ensemble member. The surface skin temperature is drawn from the model analysis dataset, and it is assumed to be the same for each ensemble member. Over water surfaces, the surface emissivity is calculated using the Meissner and Wentz (2012) model, based upon the surface skin temperature and randomly generated 10-meter wind speeds for each ensemble member. A consistent set of surface normalized radar cross sections are also generated from the ensemble of wind speeds using empirical relationships derived by Munchak et al. (2016). Over land surfaces, ensembles of surface normalized radar cross sections and

multi-spectral microwave emissivities are generated using an EOF basis for the cross sections/emissivities derived by Dr. S. Munchak (personal comm.; 2017). The EOF's of the cross sections/emissivities are randomly weighted and combined to yield ensembles of cross sections/emissivities that exhibit the natural covariability of these parameters.

Microwave brightness temperatures are calculated for each ensemble member using Eddington's second approximation with delta scaling (see Kummerow 1993; Joseph et al. 1976), which include the effects of multiple scattering of radiances. As in the multiple-scattering Ka reflectivity simulations, the mean scattering properties of the downscaled set of Ku-band profile solutions are used as input to the microwave brightness temperature simulations.

The brightness temperatures simulated in the Forward Model Module are at DPR resolution (5 km), yet the observed brightness temperatures from GMI are at lower spatial resolution (6 - 26 km). To accommodate the differences in resolutions, the observed GMI brightness temperatures are processed in the Radiance Enhancement Module to estimate brightness temperatures at the same frequencies and polarizations, but at a resolution close to the DPR resolution. Offline, a large swath of DPR-resolution brightness temperatures are simulated at all of the GMI channel frequencies and polarizations using output of the Ku Radar Module and Forward Model Module. These serve, effectively, as a set of "true" brightness temperatures at DPR resolution, and they are then convolved using the GMI antenna patterns to GMI resolution. The DPR resolution brightness temperatures are regressed against a small neighborhood of GMI-resolution brightness temperatures to create filters for the resolution enhancement of the GMI radiances. The regression procedure finds a close fit of the DPR-resolution brightness temperatures while limiting noise amplification, as in Robinson et al. (1992); see Grecu et al. (2016).

The enhancement filters are not applied directly to the GMI observations, however. Instead, they are applied to the error between the observed GMI brightness temperatures and convolved, DPR-resolution brightness temperatures from the Forward Model Module. The deconvolved errors are then used to correct the simulated, DPR-resolution brightness temperatures to estimate the most likely "observed" brightness temperatures at DPR resolution. These DPR-resolution brightness temperatures are further constrained to be within the bounds of the ensemble of simulated DPR-resolution brightness temperatures, and so the ensemble provides a physical constraint on the resolution enhancement of the GMI observations.

In the Filter Module (Fig. 2a), the Ku-reflectivity-consistent ensembles of profiles of environmental and precipitation PSD parameters are updated to be consistent with the additional information provided by the Ka-band reflectivities, PIA's, and resolution-enhanced GMI brightness temperatures. Note

that the PIA_{Ka} estimate is not used directly, but rather the rain-affected delta-PIA (PIA_{Ka} – PIA_{Ku}), which is estimated from the difference of delta-PIA at the footprint of interest and the background of Ka-Ku surface radar cross-section differences in non-raining footprints, is utilized. The rain-affected delta-PIA is provided in the output of the Radar Algorithm Level 2, and it is less corrupted by noise in the background surface cross-sections than traditional PIA estimates derived for the individual radar channels.

In the filter update procedure, any physical variable associated with the forward model could be included in the vector of unknowns, or state variables. However, for the purpose of computational efficiency, only selected variables are updated. Included in the state vector are the profiles of water vapor, $\mathbf{q_v}$, and cloud liquid, $\mathbf{q_{cld}}$, and the 10-m wind speed over water surfaces, U_{10}, as well as profile of the logarithm of the intercept of the PSD, $\log_{10}(\mathbf{N_w})$. Other variables included are the profiles of precipitation rate, **R**, and precipitation water content, **LWC**. In addition, for the purpose of testing the consistency of the brightness temperatures associated with the updated profiles relative to the GMI brightness temperatures, the DPR-resolution brightness temperatures, $\mathbf{TB_{sim}}$, are also updated. The profile of precipitation median volume diameters, $\mathbf{D_m}$, is not part of the state vector because they are derived analytically from the Ku reflectivities and *a priori* information.

An ensemble filter operator is constructed by first computing the covariances between the state variables and the simulated $\mathbf{Z_{Ka}}$, **PIA** = [PIA_{Ku}, *delta-PIA*]^T, and GMI brightness temperatures, **TB**. The covariances between the unknowns and simulated observations, combined with the actual observations, are used to update the ensemble of Ku-band solutions. Let $\mathbf{X_i}$ = [$\mathbf{q_{v\text{-}i}}$ $\mathbf{q_{cld\text{-}i}}$, $U_{10\text{-}i}$, $\log_{10}(\mathbf{N_{w\text{-}i}})$, $\mathbf{R_i}$, $\mathbf{LWC_i}$, $\mathbf{TB_{sim\text{-}i}}$]^T be a vector of the unknown parameters in the *i*th ensemble member at a given DPR footprint location. Also, let **Y** = [$\mathbf{Z_{Ka}}$ **PIA**, **TB**]^T be a vector of observed Ka-band reflectivities, path-integrated attenuations, and resolution-enhanced GMI observations, all at a given DPR footprint location. In addition, let $\mathbf{H(X_i)}$ the simulation of the observations **Y** from the unknown parameters of the *i*th ensemble member. Then, at each DPR footprint location and for each ensemble member, the EnF update, $\mathbf{X_i'}$, is given by

$$\mathbf{X_i'} = \mathbf{X_i} + \mathbf{PH^T}\left(\mathbf{HPH^T} + \mathbf{R}\right)^{-1}\left[\mathbf{Y} - \mathbf{H}\left(\mathbf{X_i}\right)\right], \tag{4}$$

where

$$\mathbf{PH^T} = \frac{1}{N-1}\sum_{i=1}^{N}\left(\mathbf{X_i} - \overline{\mathbf{X}}\right)\left[\mathbf{H}\left(\mathbf{X_i}\right) - \overline{\mathbf{H}\left(\mathbf{X}\right)}\right]^T, \tag{5}$$

$$\mathbf{HPH^T} = \frac{1}{N-1}\sum_{i=1}^{N}\left[\mathbf{H}\left(\mathbf{X_i}\right) - \overline{\mathbf{H}\left(\mathbf{X}\right)}\right]\left[\mathbf{H}\left(\mathbf{X_i}\right) - \overline{\mathbf{H}\left(\mathbf{X}\right)}\right]^T, \tag{6}$$

and

$$\mathbf{R} = \begin{bmatrix} \mathbf{W}_{Z_{Ka}} & \mathbf{0} & \mathbf{0} \\ \mathbf{0} & \mathbf{W}_{PIA} & \mathbf{0} \\ \mathbf{0} & \mathbf{0} & \mathbf{W}_{TB} \end{bmatrix} . \quad (7)$$

Here, $\mathbf{PH^T}$ is the ensemble covariance of the unknown parameters and the simulated observations, $\mathbf{HPH^T}$ is the ensemble covariance of the simulated observations, **R** is a matrix of the uncertainties in the observations, and N is the number of ensemble members. Estimated **PIA** from the surface reference technique are provided by the Radar Algorithm Level 2 output.

Equations (4)-(7) are similar to Eqs. (8)-(11) in Grecu and Olson (2008), but applied to the combined radar-radiometer estimation problem. The purpose of the update is to modify the environmental and precipitation profile parameters from the Ku-band solution to the extent that the observed $\mathbf{Z_{Ka}}$, **PIA**, and **TB** contain additional information. If the observed $\mathbf{Z_{Ka}}$ are not available or are totally attenuated by heavy rain, or if the rainfall is light (Rayleigh regime, where $Z_{Ku} = Z_{Ka}$), then the Ku-band solution will not be modified by the $\mathbf{Z_{Ka}}$, although the **PIA** and **TB** data can still alter the solution.

Equation (4) is applied to all 40 ensemble member profiles at each DPR footprint location, creating an output ensemble of μ, N_w, and D_m profiles, environmental parameters, and estimated brightness temperatures that are consistent with the observed reflectivities and path-integrated attenuations, as well as the observed brightness temperatures. The outputs of the Filter Module are ensembles of environmental/precipitation parameters and brightness temperatures consistent with both the DPR and GMI observations and their errors. The best estimate of the environmental/precipitation parameters and brightness temperatures at any DPR location is given by the mean of the filtered ensemble,

$$\overline{\mathbf{X}} = \frac{1}{N}\sum_{i=1}^{N}\mathbf{X}_i' , \quad (8)$$

and the uncertainty of the best estimate is given by the ensemble standard deviation,

$$\mathbf{s_X} = \left[\frac{1}{N-1}\sum_{i=1}^{N}\left(\mathbf{X}_i' - \overline{\mathbf{X}}\right)\left(\mathbf{X}_i' - \overline{\mathbf{X}}\right)^T\right]^{1/2} . \quad (9)$$

The uncertainty, $\mathbf{s_X}$, represents the error in the best estimate resulting from errors in the observations as well as ambiguities due to the limited information content of the observations.

Finally, for the purpose of testing the consistency of the solution brightness temperatures and the GMI observed brightness temperatures, the solution brightness temperatures are convolved by the GMI antenna patterns to create solution temperatures at GMI resolution.

Once the output of the Filter Module and the convolved solution brightness temperatures is saved to disk, the next 300 scan lines of DPR and coincident GMI data are processed, and so on, until the whole orbit is processed.

In the following subsections, the basic functions of the four primary modules of the Combined Radar-Radiometer Algorithm, including input and output parameters, are described. Supporting modules, datasets, and tables are described in section 4.

Ku Radar Module

The Ku Radar Module accepts input precipitation detection and bright band detection parameters, atmospheric environmental parameters, as well as DPR Ku reflectivity information. Its primary function is to estimate ensembles of environmental and precipitation parameters consistent with these input data at each DPR footprint location, using the generalized Hitschfeld-Bordan approach. Specifically, Radar Algorithm Level 2 input to the Ku Radar Module are precipitation detection information and calibrated Ku-band reflectivities from the Preparation Module (PRE), bright band detection and convective/stratiform classification data from the Classification Module (CSF), and environmental atmospheric pressure and temperature profiles from the Environment Module (ENV).

The Ku Radar Module also draws upon tabulated gaseous/cloud absorption coefficients and single-scattering parameters that have been pre-computed for the purpose of algorithm efficiency. Tables of gaseous absorption coefficients at Ku and Ka bands, as well as the GMI channel frequencies, are currently calculated as functions of pressure, temperature, and vapor density. Tables of cloud water/ice absorption coefficients at the same frequencies are currently calculated as functions of temperature and equivalent liquid water content; see section 4 for details.

Because precipitation of all phases produces scattering as well as absorption/emission of microwaves, and since the particle size distribution, phase, and temperature of precipitation determine its bulk scattering and absorption/emission characteristics, separate databases are used to tabulate the single-scattering properties of precipitation. In these tables, values of reflectivity, extinction coefficient, scattering coefficient, and asymmetry parameter are tabulated as functions of μ, D_m, and $\log_{10}(N_w)$, which define a normalized gamma distribution of precipitation particle sizes. Ice, liquid water, and mixed-phase particles are represented in the tables. Therefore, the Ku-band extinction and reflectivity of precipitation can be accessed from the tables in the

Ku Radar Module.

Ensembles of Ku-band consistent profiles of μ, D_m, and $\log_{10}(N_w)$ are estimated analytically in the Ku Radar Module using the generalized Hitschfeld-Bordan method. The effects of beamfilling are represented by downscaling the original observed Ku reflectivity profile to a set of lognormally-distributed reflectivity profiles, and applying the generalized Hitschfeld-Bordan method to each profile of the set.

The output of the Radar Module are ensembles of pressure, temperature, vapor density, cloud water content, μ, N_w, and D_m, precipitation rate and precipitation water content profiles, consistent with each DPR profile of Ku-band reflectivities and their uncertainties.

Forward Model Module

The Forward Model Module accepts input ensembles of profiles of environmental/precipitation parameters from the Ku Radar Module, as well as surface skin temperature and emissivity information. Its primary function is to perform forward radiative calculations of Ka-band reflectivities, path-integrated attenuations at Ku and Ka bands, and brightness temperatures at the GMI channel frequencies/polarizations, for each ensemble member profile.

In addition to the inputs from the Ku Radar Module, the Forward Model Module utilizes the static gaseous/cloud absorption and scattering tables described in the previous subsection. Based upon the input ensembles of pressure, temperature, vapor density, cloud water, μ, N_w, and D_m fields, the Forward Model Module derives the corresponding fields of single-scattering parameters for each ensemble member at the DPR and GMI channel frequencies using these tables. In addition, the surface skin temperature from the Radar Algorithm Level 2 Environment Module (ENV) and 10-meter wind speed associated with the ensembles are used to calculate the water surface emissivity, based upon the model of Meissner and Wentz (2012). Over other surfaces, emissivities are currently specified using the geographic database developed by Dr. S. Munchak (personal comm.; 2017); see section 4.

The atmospheric temperature and single-scattering properties, as well as the surface skin temperature and emissivities, at each DPR footprint location are used to simulate the Ka-band reflectivities and path-integrated attenuations at Ku and Ka bands, and they are also input to a radiative transfer model to calculate the upwelling microwave brightness temperatures at that location. To account for beamfilling effects within the radar footprint, the sets of precipitation profiles derived from the downscaled Ku-reflectivity profile in the Ku Radar Module are used to create corresponding sets of Ka reflectivity profiles that are averaged (or "upscaled") to the DPR footprint resolution. Eddington's Second Approximation, which accounts for multiple-scattering effects but which

is also computationally-efficient, is utilized to calculate the upwelling brightness temperatures; see Kummerow (1993). However, the delta scaling of bulk scattering parameters that accounts for strong forward scattering by ice-phase precipitation is also applied; see Joseph et al. (1976).

The Forward Model Module passes along the ensembles of the profiles of pressure, temperature, vapor density, cloud water content, μ, N_w, and D_m, generated by the Ku Radar Module. To these profiles, it adds ensembles of surface skin temperature, 10-meter wind speed (over water surfaces) and associated ensembles of simulated Ka-band reflectivity profiles, path-integrated attenuations at Ku and Ka bands, and surface emissivities and upwelling brightness temperatures at the GMI channel frequencies/polarizations.

Radiance Enhancement Module

The Radiance Enhancement Module receives convolved, simulated brightness temperature ensembles from then Forward Model Module and observed GMI brightness temperatures from the Radiometer Algorithm Level 1C as inputs. It estimates near-DPR-resolution GMI brightness temperatures using a regression-based filter, and outputs these enhanced-resolution brightness temperatures. It also passes along the ensembles of profiles of pressure, temperature, vapor density, cloud water content, μ, N_w, and D_m, precipitation rates and precipitation water contents, surface skin temperatures and 10-meter wind speeds (over water surfaces), and simulations of surface emissivities and upwelling brightness temperatures, generated by previous Modules.

Filter Module

The Filter Module ingests the ensembles of environmental and precipitation parameters as well as the simulated Ka-band reflectivities, path-integrated attenuations at Ku and Ka bands, and surface emissivities and upwelling brightness temperatures at the GMI channel frequencies/polarizations. It also requires observed Ka-band reflectivities, path-integrated attenuations at Ku and Ka bands, as well as the resolution-enhanced GMI observations from the Radiance Enhancement Module, as input. Its primary function is to filter the profile ensembles to create updated profile ensembles that are consistent with all valid DPR and GMI observations, and their uncertainties. Based on the updated ensembles, it also computes "best estimates" of the precipitation parameters and their uncertainties.

Specifically, the Filter Module uses the covariances between the input ensemble profiles and the simulated observations from the Forward Model Module, and combines these with actual observations of Ka-band reflectivities, path-integrated attenuations at Ku and Ka bands, and resolution-enhanced GMI brightness temperatures to perform an ensemble filter update of the input ensembles of precipitation parameter profiles. The brightness temperature ensembles are also filtered for the purpose of evaluating the fitting of the

simulated brightness temperatures to the observed brightness temperatures. Ka-band reflectivities are drawn from the Radar Algorithm Level 2 Preparation (PRE) Module, and Ku/Ka path-integrated attenuation observations are taken from the Radar Algorithm Level 2 Surface Reference Technique (SRT) Module. GMI brightness temperatures are drawn from the Radiance Enhancement Module output of observed brightness temperature data that have been resolution-enhanced to near-DPR resolution. Details of the ensemble filtering method may be found in Grecu and Olson (2008), Grecu et al. (2011), and Grecu et al. (2016).

Output of the Filter Module includes best estimates of the environmental parameters, such as profiles of vapor density and cloud liquid water, as well as estimates of 10-meter wind speed. With respect to precipitation, profiles of precipitation size distribution parameters (μ, N_w, D_m), precipitation rate and water content, as well as surface precipitation rate are estimated. In addition, the fractions of liquid in the profiles of precipitation water content and precipitation rate and surface precipitation rate are output. Estimates of the uncertainties of the precipitation rates and water contents, as well as uncertainties of surface precipitation rates, are produced. Also output are by-products of the estimation method, including profiles of corrected radar reflectivity factor at Ku and Ka bands, and the estimated path-integrated attenuation at Ku and Ka bands and surface emissivities/brightness temperatures at the GMI channel frequencies/ polarizations.

4. Ancillary Datasets

In the current algorithm formulation, only the Analysis Data, described below, are ingested from an external source during Combined Algorithm processing. The other databases and tables are static and are read into memory upon the execution of the algorithm software.

Geographic Data

A geographic database containing water coverage and elevation information at 5 km resolution is required by the Combined Algorithm; see section 3. Water fractions in the database are derived from the Moderate Resolution Imaging Spectroradiometer (MODIS) 250 m resolution land-water mask, and elevations are derived from the Shuttle Radar Topography Mission 30" (SRTM30) data, both re-projected to the NASA Land Information System (LIS) 1 km grid. Finally, the 1 km resolution data are averaged to 5 km to match the resolution of the DPR.

Analysis Data

Analysis data are required to produce initial estimates of environmental parameters such as pressure, temperature, and surface skin temperature. The current algorithm design requires space-time interpolation of these data from the Japanese Meteorological Agency's (JMA) global analyses (GANAL) during

standard algorithm processing. The data are interpolated to the DPR footprint/range bin locations and overpass times in the Environment Module (ENV) of the Radar Algorithm Level 2 and then output. For near real-time processing, the JMA analysis is supplemented with JMA forecast fields, but if these fields are not received in time for any reason, Japanese 25-year Re-analysis (JRA-25) data are substituted for the JMA analysis/forecast data in the ENV processing.

Data Supporting the Specification of Environmental Parameters

Atmospheric vapor density and cloud water content profiles utilized in the creation of the *a priori* profile ensembles are derived from random combinations of EOF's that are based upon cloud-system-resolving model simulations. The EOF's are drawn from Weather Research and Forecasting model (WRF, Michalakes et al. 2001) simulations representing diverse meteorological systems (e.g. mid-latitude cyclones, tropical convection, etc.). Cloud ice is currently not represented in the Combined Algorithm.

Water surface emissivities are modeled as a function of surface skin temperature and 10-meter wind speed over water surfaces (Meissner and Wentz 2012. These emissivities are empirically related to surface normalized radar cross sections by Munchak et al. (2016). Land surface emissivities and

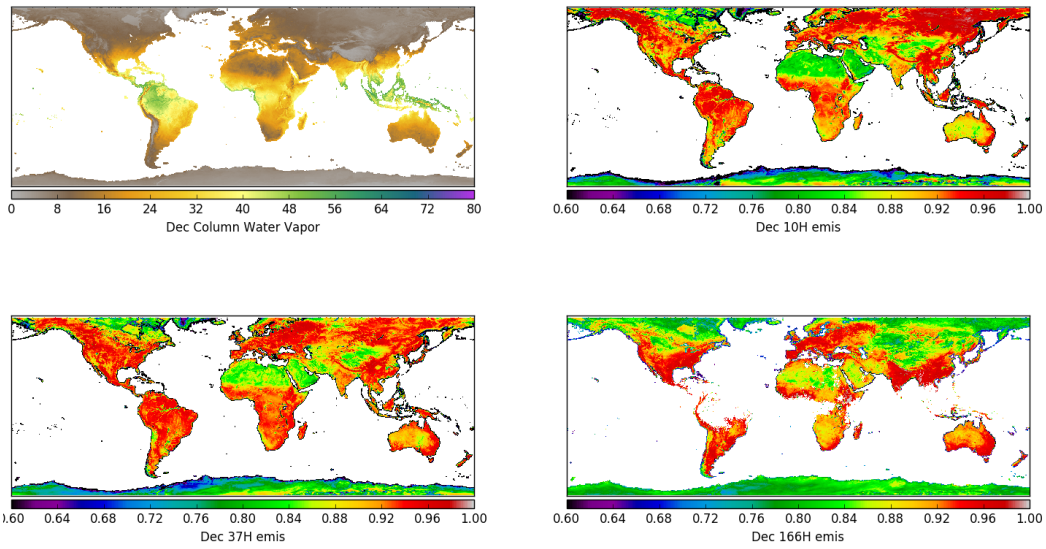

Fig. 3. Mean column water vapor (upper left) and surface emissivities at 10 GHz (upper right), 37 GHz (lower left), and 166 GHz (lower right) in the horizontal polarization for the month of December, derived by Dr. S. Munchak (personal comm., 2017). Missing data in high cloudiness areas are due to a lack of an adequate uncontaminated radiance sample in those areas.

normalized radar cross sections are derived from the geographic empirical database developed by Dr. S. Munchak (personal comm.; 2017). Examples of monthly-mean land surface emissivities in the horizontal polarization are shown in Fig. 3.

Microwave Absorption and Single-Scattering Tables

Two types of tables are produced by the GPM Radar Algorithm and Combined Algorithm Teams. The first table type contains microwave absorption coefficients for atmospheric gaseous constituents indexed by pressure, temperature, and humidity, and also cloud water/ice absorption coefficients indexed by temperature and liquid-equivalent cloud water content. Tables of gaseous absorption coefficients at Ku and Ka bands, as well as the GMI channel frequencies, are currently calculated as functions of pressure, temperature, and vapor density using the model described in Rosenkranz (1998). Tables of cloud water/ice absorption coefficients at the same frequencies are currently calculated as functions of temperature and equivalent liquid water content using Mie theory.

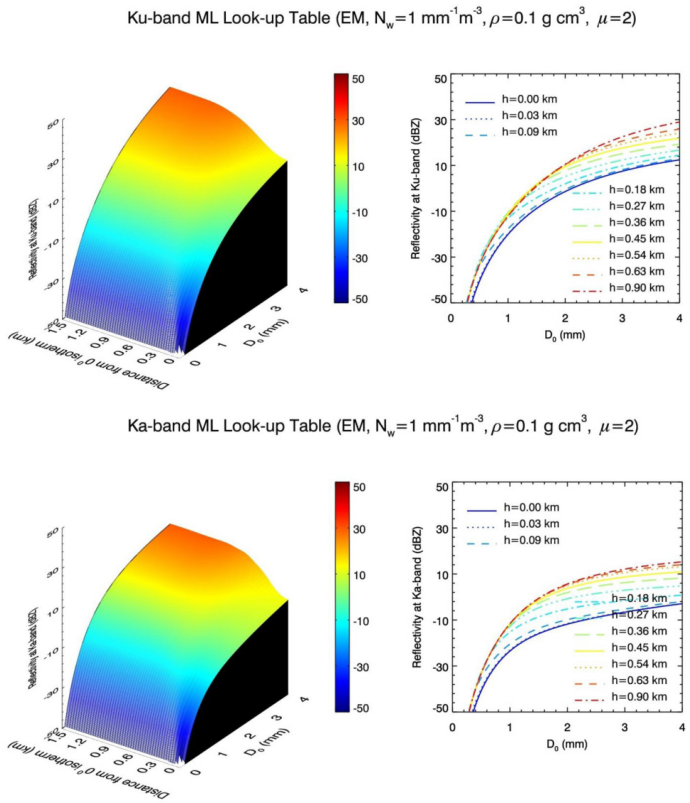

Fig. 4. Graphical illustrations of Ku-band (top) and Ka-band (bottom) scattering table entries for radar reflectivities within the melting layer. Color plots show the variation of reflectivity (given N_w) with both D_o and distance below the 0°C level. Line plots show the same information for specific depths below the 0°C level.

Because precipitation of all phases induces scattering as well as absorption/emission of microwaves, and since the particle size distribution,

phase, and temperature of precipitation determine its bulk (size distribution integrated) scattering and absorption/emission characteristics, separate tables are used to store the single-scattering properties of precipitation. This second table type contains bulk reflectivities, extinction coefficients, scattering coefficients, and asymmetry parameters of precipitation at Ku and Ka bands, as well as the GMI channel frequencies. The bulk scattering parameters are derived by integrating the single-scattering properties of precipitation particles over assumed gamma distributions of particles, indexed by μ, N_w, and D_m, which define the normalized gamma distribution. Separate tables are generated for precipitation at different temperatures. In addition, for mixed-phase precipitation in stratiform regions, tables are also created for different vertical displacements relative to the freezing level.

To estimate the single-scattering properties of raindrops, all drops are assumed to be spherical liquid particles, and Mie theory is applied to obtain the scattering properties of the drops. Mixed-phase particles are assumed to be concentric shells of ice, air, and liquid water, for which the ice-air density is 0.1 g cm^{-3}. The proportion of liquid water in each shell is assumed to increase with radius within the particle according to an analytical formula (Liao and Meneghini, 2005), summing to a prescribed total melt fraction. In stratiform regions the total melt fraction is determined using a thermodynamic melting simulation; see Yokoyama and Tanaka (1984), while in convective regions the melt fraction is assumed to vary linearly from 0 at the top of the mixed-phase region to 1 at the its base. Multi-shell electromagnetic theory is used to compute the single-scattering properties of the mixed-phase particles; see Wu and Wang (1991). A graphical illustration of entries for the mixed-phase precipitation type is shown in Fig. 4 for Ku- and Ka-band reflectivities of melting snow particle distributions at various depths below the freezing level. Ice-phase precipitation particles are assumed to be nonspherical, computationally simulated as aggregates of pristine crystals, as described in Kuo et al. (2016). The single-scattering properties of the nonspherical ice particles are derived using the discrete dipole approximation; see Draine and Flatau (1994).

5. Summary of Algorithm Input/Output

Input to the Combined Algorithm is derived from Radar Algorithm Level 2 (2AKu, 2AKuENV, 2ADPR) products and from the Radiometer Algorithm Level 1C GMI (1CGMI) product, as well as the ancillary datasets described in section 4.

The output of the Combined Algorithm is the 2BCMB product, which contains two swaths of data. Precipitation estimates in the NS output swath are derived from coincident DPR Ku band reflectivities/PIA's and GMI brightness temperatures, and these estimates will extend across the entire Ku band swath. Precipitation estimates in the MS output swath are derived from coincident DPR Ku- and Ka-band reflectivities/PIA's and GMI brightness temperatures. The MS

precipitation estimates are therefore limited to the DPR Ku-Ka overlap swath. Since the MS swath estimates draw upon the maximum amount of information from the GPM Core sensors, these estimates will be the main tool for cross-calibrating the GPM constellation radiometer precipitation estimates through the creation of *a priori* databases. The same Combined Algorithm software architecture is used to create both the NS or MS output swaths.

A complete listing of Combined Algorithm input/output parameters is included in Appendix A. Output volumes and algorithm processing requirements are included in Appendix B and C, respectively.

6. Algorithm Testing Plan

Prior to the GPM Core Observatory launch, testing of the Combined Algorithm or Algorithm components fell into three categories: Sensitivity Testing, Physics Testing, and Pre-launch Validation. After GPM Core launch, Sensitivity Testing and Physics Testing continued, and Pre-launch Validation activities evolved into Post-launch Validation.

Sensitivity Testing

Sensitivity tests basically quantify the impact of different algorithm modifications on output products. So, it is possible that even if the Combined Algorithm investigators suspect that a particular algorithm modification should have a significant impact based upon previous work or intuitive reasoning, that modification may actually have little impact or an impact that was not foreseen. Sensitivity testing can therefore be used to prioritize or re-focus areas of algorithm development based upon the specific impact algorithm modifications have on output.

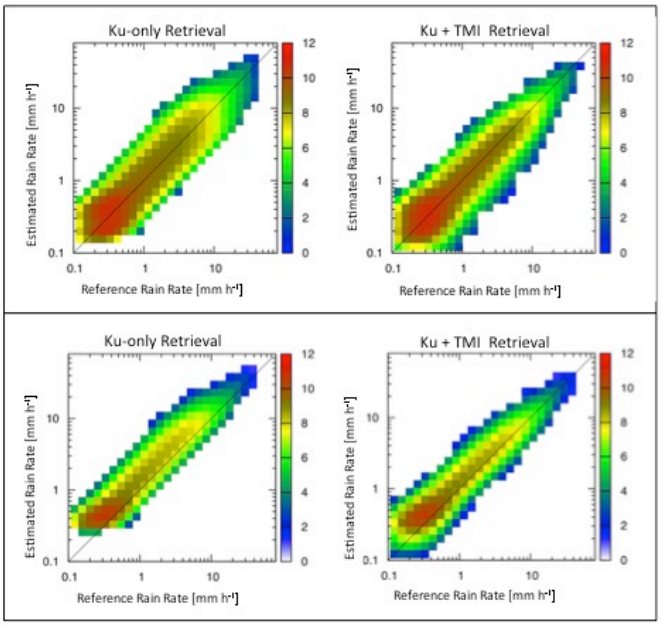

Fig. 5. Shown in the top panels are 2D histograms of synthetic retrievals of surface rain rate vs. reference rain rates, using only Ku band input data (left panel) and using both Ku band and TMI input data (right panel). The bottom panels are the same, except that the mean of the initial guess N_w values is assumed to be 4x the mean of the actual reference values.

Input data for sensitivity testing can vary depending on the algorithm modification. Typically, we use Ku band radar data from either airborne sensors or TRMM observations to synthesize Ka band radar reflectivity and GMI brightness temperature observations. In this way we can ensure physical consistency between the radar and radiometer channels using the same forward modeling assumptions. The following are some ongoing and planned areas of sensitivity testing:

- impact of changes in algorithm methodology
- impact of different input data (e.g., radar vs. radar-radiometer)
- impact of PSD description
- impact of assumed environmental/precipitation parameter correlations
- impact of particle scattering assumptions
- impact of precipitation phase transition assumptions
- impact of land surface characterization and physical parameterizations
- impact of source of ancillary (analysis) data
- impact of radar non-uniform beamfilling assumptions
- impact of radar multiple-scattering effects

This list is by no means exhaustive.

An example of sensitivity testing is the study of the impact of DPR and GMI input data on Combined Algorithm estimates relative to estimates based upon the DPR input data alone. Shown in Fig. 5 are 2D histograms (similar to scatterplots) of estimated surface rainfall rates from algorithm applications to

synthetic data versus the known reference rainfall rates. Only the Ku band reflectivity data are utilized in the algorithm applications illustrated on the left-hand side of the figure, while both Ku band and TMI brightness temperature data are utilized in the algorithm applications illustrated on the right-hand side. If the initial guess ensemble of N_w values has the same mean as the reference values, then the addition of the TMI observations reduces the scatter of estimated rainfall rates relative to the reference values. If the initial guess ensemble of N_w values is biased by a factor of 4 relative to the reference values, there is a greater bias correction if both the Ku band and TMI observations are utilized.

Sensitivity testing is expected to be a long-term activity that will help us to improve our understanding of the Combined Algorithm's response to a variety of potential modifications.

Physics Testing

The objective of Physics Testing is to verify assumptions in the forward models that relate environmental/precipitation parameters to sensor observations. Since the current TRMM and GPM radars and radiometers have relatively low resolution, field campaign observations from airborne and ground-based instrumentation generally provide superior data for physics testing. These data may include remote sensing radar and radiometer observations as well as *in situ* measurements.

Ongoing or planned areas of physics testing include

- assessment of appropriate physical models for ice-phase precipitation
- assessment of proper parameterizations for the ice-to-liquid phase transition
- assessment of appropriate physical models for mixed-phase precipitation
- assessment of physical models for land surface emissivities
- assessment of parameterizations for describing inhomogeneity of precipitation within the radar footprint
- assessment of physical parameterizations for multiple scattering of radar pulses

Fig. 6 illustrates a precursor of physics testing to determine appropriate physical parameterizations of ice-phase precipitation in the Combined Algorithm. In this test, different physical models are assumed for describing the single-scattering properties of ice-phase precipitation in a precipitation estimation algorithm. The estimation algorithm is applied to Dual-frequency Airborne Precipitation Radar (APR-2) Ku and Ka band observations from the

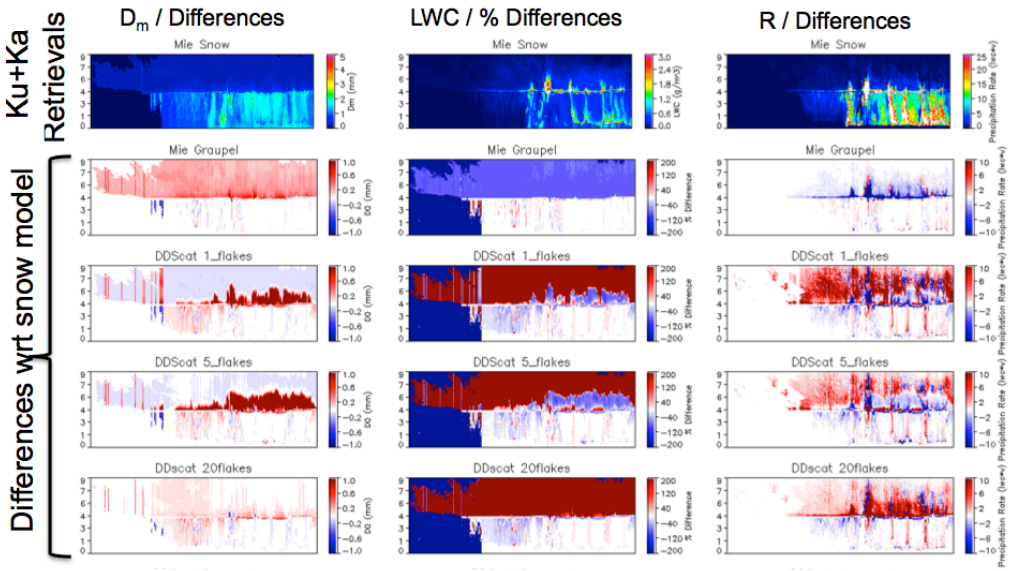

Fig. 6. Top row are estimated mass-weighted mean diameter, D_M, liquid water content, LWC, and rain rate, R, based upon airborne APR-2 Ku and Ka band radar data. Ice-phase precipitation is assumed to be spherical snow particles with mixed ice-air dielectric properties. Shown in the second row are the differences between Ku/Ka band estimates assuming spherical, mixed-dielectric graupel particles and mixed-dielectric snow particles. Shown in the third, fourth, and fifth rows are the differences between estimates assuming structured snow particles composed of multiple dendritic flakes and spherical mixed-dielectric snow particles.

Genesis and Rapid Intensification Processes (GRIP) field campaign. The reflectivity observations (not shown) indicate a stratiform precipitation region with embedded convective elements. It is evident from the figure that the choice of ice-phase precipitation scattering model has an impact on the estimation of the precipitation mass-weighted particle diameter, water content, and rainfall rate.

During the Midlatitude Continental Convective Clouds Experiment (MC3E), the GPM Cold-season Precipitation Experiment (GCPEX), the Integrated Precipitation and Hydrology Experiment (IPHEx), and the Olympic Mountains Experiment (OLYMPEX), airborne dual-frequency radar observations are coupled with coincident microwave brightness temperature measurements and *in situ* microphysics probe observations of precipitation. The precipitation algorithm will be applied to these combined radar-radiometer data to see if

reasonable fits to the data can be achieved, and to see if agreement with *in situ* observations is possible, given different assumed ice scattering parameterizations.

Physics testing is expected to be a long-term activity that will help us to improve our understanding of the Combined Algorithm's forward model and its uncertainties.

Pre-launch Validation

Prior to the GPM Core Observatory launch, the Combined Algorithm was examined to determine (a) in TRMM applications, how Combined Algorithm precipitation estimates compared to TRMM V7 Algorithm estimates and well-calibrated ground-based radar estimates, and (b) whether or not Combined Algorithm estimates would be expected to meet the GPM Level-1 Science Requirements. It is stated in the Science Requirements that the algorithm should be capable of estimating instantaneous surface rainfall rates at 50 km resolution with a bias and random error within 50% at 1 mm h^{-1} rain rate and within 25% at 10 mm h^{-1} rain rate.

With respect to TRMM applications, the Combined Algorithm performance should be similar to what might be expected outside the GPM Ka band swath, where only Ku band and GMI brightness temperature observations are available. Shown in Fig. 7 are preliminary comparisons of surface rain rate estimates from the TRMM V7 Radar Algorithm (2A25), the TRMM V7 Combined Algorithm (2B31), and the GPM prototype Combined Algorithm (EnF). Note the general similarity between the rain rate estimates, which is attributed to the similar physical basis of all three algorithms.

Although coincident ground-based radar observations were not available for the precipitation systems shown in Fig. 7, well calibrated radar with raingages sited within the radar observing domain were available from the Melbourne, Florida and Kwajalein Atoll, Republic of Marshall Islands ground validation sites; see Wolff et al. (2005). Both sites feature S-band, nearly non-attenuating radars; the KPOL radar at Kwajalein is polarimetric and the Melbourne WSR-88D radar was upgraded to polarimetric in January, 2012. Polarimetric capability helps to improve quality control of the data and provide more definitive rain rate estimates. These high quality ground validation estimates will be compared to Combined Algorithm estimates to provide evidence for whether or not the Science Requirements will be met by the algorithm.

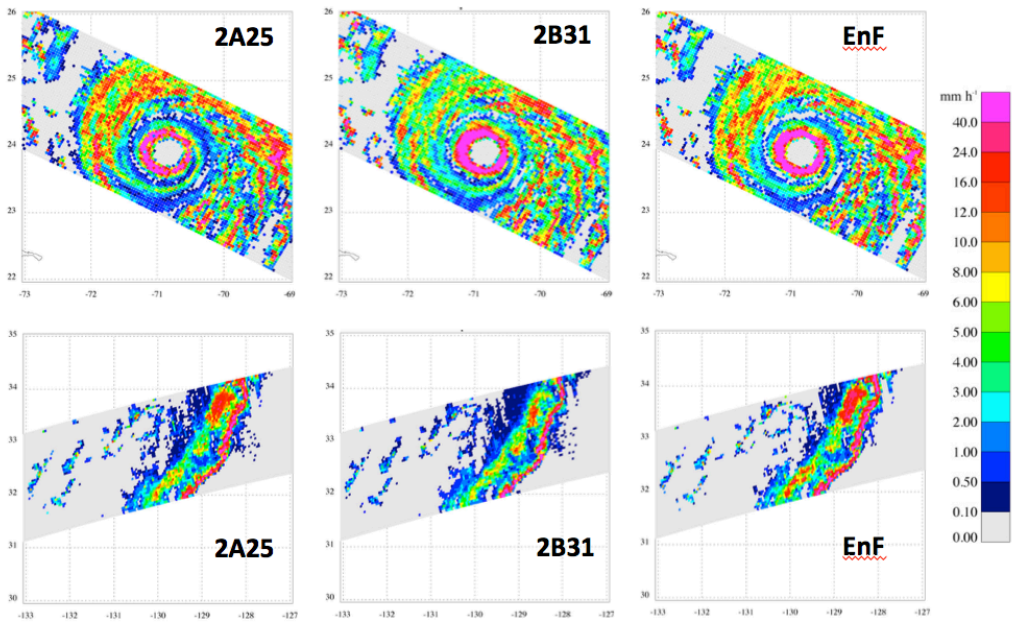

Fig. 7. Top row, estimated surface rainfall rates in Tropical Cyclone Floyd at 09 UTC 13 September 1999 from the TRMM V7 2A25 (radar-only), TRMM V7 2B31 (radar-radiometer) and TRMM EnF (prototype GPM radar-radiometer) algorithms. Bottom row, same as top row but TRMM estimates are for a wintertime cold frontal band over the Eastern Pacific Ocean at 00 UTC 19 February 2001.

In addition, the GPM Validation Network (VN) and Multi-Radar Multi-Sensor (MRMS) quantitative precipitation estimation product formerly called NMQ, will provide large-scale coverage of three dimension reflectivity distributions and surface rainfall rates, respectively, for identifying locally large discrepancies between satellite and ground-based measurements. Both products are based upon the US NEXRAD radar network. The VN network covers the continental US and several sites outside the US, and these reflectivity data are geometrically "matched" to reflectivity observations from the TRMM PR and GPM DPR; see Schwaller and Morris (2011). Of particular interest is how well the attenuation corrected reflectivities from the Combined Algorithm agree with the VN S-band reflectivities, that are essentially unaffected by attenuation. To do these intercomparisons properly, a small Mie correction is applied to the Combined estimates of attenuation-corrected Ku band reflectivities; see Liao and Meneghini (2009). The NOAA MRMS product is a 1 km, 5 minute resolution instantaneous rain rate product derived from the National Weather Service NEXRAD radar network and Environment Canada radars in lower Canada, as well as coincident raingages; see Kirstetter et al. (2012). Like the VN, the MRMS data have the advantage of broad spatial coverage, with observations extending over the continental US starting in 2006.

Post-launch Validation

Now that the GPM Core Observatory has been put into orbit and calibration adjustments are nearly complete, ground validation of Combined Algorithm estimates of precipitation continues using data from well calibrated and monitored ground radar data from sites such as Kwajalein, Dallas/Fort Worth, and Houston. These sites will be augmented with observations from NASA's NPOL radar and supporting raingage network at NASA Wallops Flight Facility, as well as higher-latitude sites in Finland, Canada, and S. Korea. The US NEXRAD Network has been completely upgraded to dual-polarization, leading to improved accuracy of quantitative precipitation estimates from the MRMS and VN. Validation strategies are much the same as those used to evaluate TRMM-based algorithm estimates in the Pre-launch era; see the preceding subsection.

Shown in Fig. 8 are scatterplots of instantaneous, 0.5° resolution Combined Algorithm V5 estimates of surface precipitation rate vs. MRMS gage-calibrated radar precipitation rates over the continental US from the period Sep. 2014 – Aug. 2015. The MRMS precipitation rates are matched to the Combined Algorithm resolution footprints (5 km resolution) and binned with the Combined Algorithm estimates in 0.5° x 0.5° boxes. Note that there is a slight increase in the correlation of Combined Algorithm MS estimates relative to NS estimates.

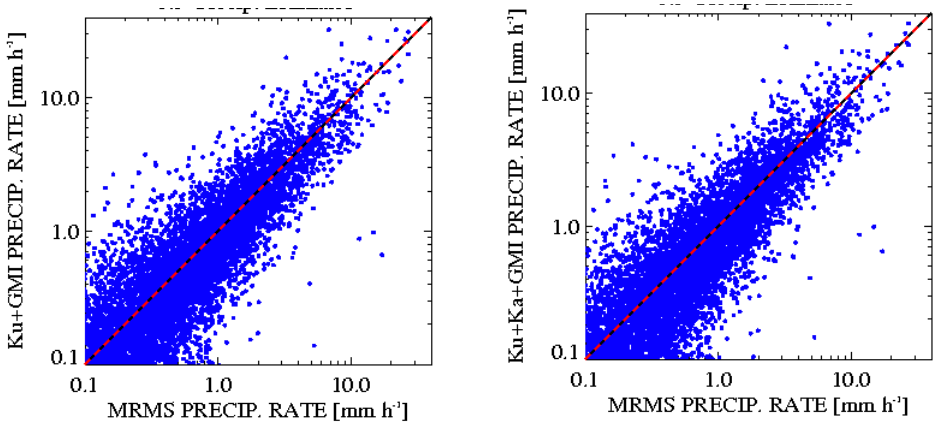

Fig. 8. Scatterplots of instantaneous, 0.5° resolution NS mode (Ku+GMI; at left) and MS mode (Ku+Ka+GMI; at right) estimates of surface precipitation rates vs. MRMS raingage-calibrated radar estimates for the period Sep. 2014 – Aug. 2015. The correlation of NS mode precipitation rates is 0.85, while the correlation of MS mode estimates is 0.86.

Global distributions of Combined Algorithm MS mode (Ku+Ka+GMI) estimates of surface precipitation rate and Global Precipitation Climatology Project (GPCP) estimates and their differences, along with corresponding zonal mean rain rate distributions, for the period Sep. 2014 – Aug. 2015, are shown in Fig. 9. Note that the Combined Algorithm and GPCP distributions are similar,

with the most obvious differences at the high latitudes. At high latitudes, the weak signal of low-density, ice-phase precipitation may not be detectable by the DPR, and alternative strategies for estimating precipitation with the radar-radiometer combination are now being pursued for those cold regimes. Fluctuations of differences at lower latitudes are partly due to sampling differences of the narrow-swath MS product and the GeoIR-based GPCP, but some biases of MS over land are evident. These biases are the subject of current algorithm investigations.

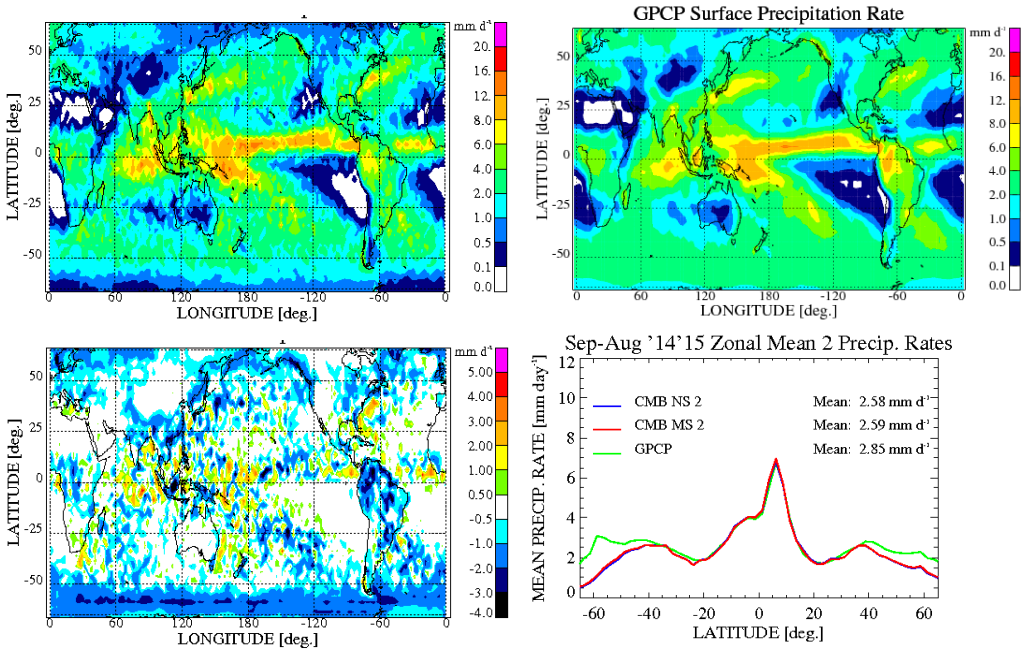

Fig. 9. Global mean precipitation distributions from the Combined Algorithm MS mode (Ku+Ka+GMI; upper left) and GPCP (upper right), the MS – GPCP difference (lower left), as well as zonal means (lower right), for the period Sep. 2014 – Aug. 2015.

Metrics

As shown in Olson et al. (2006), the use of instantaneous, 50 km resolution rain rate estimates represents a reasonable compromise in resolution for evaluating algorithm errors. Although validation at resolutions down to 5 km (the nominal DPR resolution) may be attempted, the influence of satellite vs. ground radar collocation errors degrades any derived statistics. Accumulation of the 50-km estimates over seasons can reveal spatial patterns of bias (relative to reference estimates) that are helpful for diagnosing systematic algorithm errors.

Standard bivariate statistics of the "errors" between Combined Algorithm rain estimates and ground-based estimates, such as the mean error (bias), error standard deviation, and correlation coefficient will be computed, generally stratified by the rain intensity. These statistics can be used to assess the

algorithm's performance relative to the Level 1 Science Requirements, for example. However, information more relevant to algorithm improvement can be gained if the statistics are stratified by other variables that indicate specific state dependencies of the error. For example, are the errors functions of surface skin temperature, total precipitable water, or other variables that indicate the climate regime, or, are the errors functions of the precipitation system or type, such as the convective/stratiform class? Stratification of statistics to reveal state dependencies of algorithm error will be important for diagnosing algorithm deficiencies, especially in the early phases of the GPM Core mission.

In addition to meeting the L1 Science Requirements, a measure of the success of our effort will be the quantification of any improvements in combined radar-radiometer estimates relative to radar-only estimates within the GPM Combined Algorithm framework.

7. References

Aires, F., C. Prigent, F. Bernardo, C. Jimenez, R. Saunders, and P. Brunel, 2011: A Tool to Estimate Land Surface Emissivities in the Microwave (TELSEM) for use in numerical weather prediction. *Quart. J. Royal Meteorol. Soc.*, **137**, 690-699.

Anderson, J. L., 2003: A local least squares framework for ensemble filtering. *Mon. Wea. Rev.*, **131**, 634-642.

Battaglia, A., S. Tanelli, K. Mroz, and F. Tridon, 2015: Multiple scattering in observations of the GPM dual-frequency precipitation radar: Evidence and impact on retrievals. *J. Geophys. Res. Atmos.*, **120**, 4090-4101.

Draine, B. T., and P. J. Flatau, 1994: Discrete-dipole approximation for scattering calculations. *J. Opt. Soc. Am. A*, **11**, 1491-1499.

Grecu, M., and W. S. Olson, 2008: Precipitating snow retrievals from combined airborne cloud radar and millimeter-wave radiometer observations. *J. Appl. Meteor. and Climatol.*, **47**, 1634-1650.

Grecu, M., L. Tian, W. S. Olson, and S. Tanelli, 2011: A robust dual-frequency radar profiling algorithm. *J. Appl. Meteor. and Climatol.*, **50**, 1543-1557.

Grecu, M., W. S. Olson, S. J. Munchak, S. Ringerud, L. Liao, Z. S. Haddad, B. L. Kelley, and S. F. McLaughlin, 2016: The GPM Combined Algorithm. *J. Atmos. and Oceanic Tech.*, **33**, 2225-2245.

Hogan, R. J., and A. Battaglia, 2008: Fast lidar and radar multiple-scattering models. Part II: Wide-angle scattering using the time-dependent two-stream approximation. *J. Atmos. Sci.*, **65**, 3636-3651.

Joseph, J. H., W. J. Wiscombe, and J. A. Weinman, 1976: The delta-Eddington approximation for radiative flux transfer. *J. Atmos. Sci.*, **33**, 2452-2459.

Kirstetter, P.-E., Y. Hong, J. J. Gourley, S. Chen, Z. Flamig, J. Zhang, M. Schwaller, W. Petersen, and E. Amitai, 2012: Toward a framework for systematic error modeling of spaceborne precipitation radar with NOAA/NSSL ground radar-based national mosaic QPE. *J. Hydrometeorol.*, **13**, 1285-1300.

Kummerow, C., 1993: On the accuracy of the Eddington Approximation for radiative transfer in the microwave frequencies. *J. Geophys. Res. – Atmos.*, **98**, 2757-2765.

Kuo, K.-S., W. S. Olson, B. T. Johnson, M. Grecu, L. Tian, T. L. Clune, B. H. van Aartsen, A. J. Heymsfield, L. Liao, and R. Meneghini, 2016: The microwave radiative properties of falling snow derived from nonspherical ice particle models. Part I: An extensive database of simulated pristine crystals and aggregate particles, and their scattering properties. *J. Appl. Meteor. and Climatol.*, **55**, 691-708.

Liao, L., and R. Meneghini, 2005: On modeling air/spaceborne radar returns in the melting layer. *IEEE Trans. Geosci. Remote Sens.*, **43**, 2799 - 2809.

Liao, L., and R. Meneghini, 2009: Changes in the TRMM Version-5 and Version-6 Precipitation Radar products due to orbit boost. *J. Met. Soc. Japan*, **87A**, 93-107.

Meissner, T., and F. J. Wentz, 2012: The emissivity of the ocean surface between 6 and 90 GHz over a range of wind speeds and earth incidence angles. *IEEE Trans. Geosci. Remote Sens.*, **50**, 3004-3026.

Meneghini, R., T. Iguchi, T. Kozu, L. Liao, Ken'Ichi Okamoto, J. A. Jones, and J. Kwiatkowski, 2000: Use of the Surface Reference Technique for path attenuation estimates from the TRMM Precipitation Radar. *J. Appl. Meteor.*, **39**, 2053-2070.

Michalakes, J., S. Chen, J. Dudhia, L. Hart, J. Klemp, J. Middlecoff, and W. Skamarock, 2001: Development of a next generation regional weather research and forecast model. *Developments in Teracomputing: Proceedings of the Ninth ECMWF Workshop on the Use of High Performance Computing in Meteorology*, W. Zwieflhofer and N Kreitz, Eds., World Scientific, 269-276.

Munchak, S. J., R. Meneghini, M. Grecu, and W. S. Olson, 2016: A consistent treatment of microwave emissivity and radar backscatter for retrieval of precipitation over water surfaces. *J. Atmos. Oceanic Tech.*, **33**, 215-229.

Olson, W. S., C. D. Kummerow, S. Yang, G. W. Petty, W.-K. Tao, T. L. Bell, S. A. Braun, Y. Wang, S. E. Lang, D. E. Johnson and C. Chiu. 2006: Precipitation and latent heating distributions from satellite passive microwave radiometry. Part

I: Improved method and uncertainties. *J. Appl. Meteor. and Climatol.*, **45**, 702–720.

Prigent, C., F. Aires, and W. B. Rossow, 2006: Land surface microwave emissivities over the globe for a decade. *Bull. Amer. Met. Soc.*, **87**, 1573-1584.

Robinson, W. D., C. Kummerow, and W. S. Olson, 1992: A technique for enhancing and matching the resolution of microwave measurements from the SSM/I instrument. *IEEE Trans. Geosci. Remote Sens.*, **30**, 419-429.

Rosenkranz, P. W., 1998: Water vapor microwave continuum absorption: A comparison of measurements and models. *Radio Sci.*, **33**, 919-928.

Schwaller, M. R., and K. R. Morris, 2011: A ground validation network for the Global Precipitation Measurement Mission. *J. Atmos. Oceanic Tech.*, **28**, 301-319.

Testud, J., S. Oury, P. Amayenc, and R. A. Black, 2001: The concept of normalized distributions to describe raindrop spectra: A tool for cloud physics and cloud remote sensing. *J. Appl. Meteor.*, **40**, 1118–1140.

Thompson, E. J., S. A. Rutledge, B. Dolan, and M. Thurai, 2015: Drop size distributions and radar observations of convective and stratiform rain over the equatorial Indian and West Pacific Oceans. *J. Atmos. Sci.*, **72**, 4091-4125.

Wolff, D. B., D. A. Marks, E. Amitai, D. S. Silberstein, B. L. Fisher, A. Tokay, J. Wang, and J. L. Pippitt, 2005: Ground validation for the Tropical Rainfall Measuring Mission (TRMM). *J. Atmos. Oceanic Tech.*, **22**, 365-380.

Wu, Z. S., and Y. P. Wang, 1991: Electromagnetic scattering for multilayered sphere: Recursive algorithms. *Radio Sci.*, **26**, 1393-1401.

Yokoyama, T., and H. Tanaka, 1984: Microphysical process of melting snowflakes detected by two-wavelength radar. *J. Met. Soc. Japan*, **62**, 650-666.

Appendix A. Listing of Input/Output Parameters

Input Parameters
This listing includes only those parameters that will be ingested from GPM Algorithms that are external to the Combined Radar-Radiometer Algorithm code. The given array size arguments correspond to:

nscan = number of DPR scans per granule, approximately 7900
nray = 49 rays of Normal Swath (NS) Ku band data
nrayMS = 25 rays of Matched Swath (MS) Ka band data
nrayHS = 24 rays of High sensitivity Swath (HS) Ka band data
nbin = 176 range bins of NS or MS radar data per ray
nbinHS = 88 range bins of HS Ka band data per ray
method = 6 methods for estimating path-integrated attenuation from the SRT
nNode = 5 bin nodes identified in the radar-defined DSD structure
nwind = 2 wind components: u, v
nwater = 2 water vapor and cloud liquid water profile parameters

nscan1 = number of lower-frequency (S1) GMI scans in the granule, approx. 2954
nscan2 = number of higher-frequency (S2) GMI scans in the granule, approx. 2954
npixel1 = 221 pixels per lower-frequency (S1) GMI scan
npixel2 = 221 pixels per higher-frequency (S2) GMI scan
nchannel1 = 9 channels of lower-frequency (S1) GMI data per pixel
nchannel2 = 4 channels of higher-frequency (S2) GMI data per pixel
nchUIA1 = 1 number of lower-frequency (S1) unique incidence angles
nchUIA2 = 1 number of higher-frequency (S2) unique incidence angles

from the 2AKu Radar Algorithm

Year
year of the Ku scan (2 byte integer, nscan); from the 2AKu Radar Algorithm.

Month
month of the Ku scan (1 byte integer, nscan); from the 2AKu Radar Algorithm.

DayOfMonth
day of month of the Ku scan (1 byte integer, nscan); from the 2AKu Radar Algorithm.

Hour
hour of the Ku scan (1 byte integer, nscan); from the 2AKu Radar Algorithm.

Minute
minute of the Ku scan (1 byte integer, nscan); from the 2AKu Radar Algorithm.

Second
second of the Ku scan (1 byte integer, nscan); from the 2AKu Radar Algorithm.

MilliSecond
millisecond of the Ku scan (2 byte integer, nscan); from the 2AKu Radar Algorithm.

DayOfYear
day of the year of the Ku scan (2 byte integer, nscan); from the 2AKuRadar Algorithm.

SecondOfDay
second of the day of the Ku scan (8 byte float, nscan); from the 2AKu Radar Algorithm.

Latitude
latitude of Ku footprint (4 byte float, nray x nscan); from the 2AKu Radar Algorithm.

Longitude
longitude of Ku footprint (4 byte float, nray x nscan); from the 2AKu Radar Algorithm.

elevation
altitude above the Earth ellipsoid of the surface gate in Ku ray (4 byte float, nray x nscan); from the 2AKu Radar Algorithm (PRE Module).

landSurfaceType
water/land/coast and surface type at Ku footprint location (4 byte integer, nray x nscan); from the 2AKu Radar Algorithm (PRE Module). Note that this information is used to interpret surface reference technique output.

localZenithAngle
local incidence angles of DPR ray relative to local zenith on the Earth ellipsoid (4 byte float, nray x nscan); from the 2AKu Radar Algorithm (PRE Module).

flagPrecip
flag indicating detection of precipitation or no precipitation in Ku ray (4 byte integer, nray x nscan); from the 2AKu Radar Algorithm (PRE

Module).

binRealSurface
surface range bin in Ku ray (2 byte integer, nray x nscan); from the 2AKu Radar Algorithm (PRE Module).

binStormTop
range bin of storm top in Ku ray (2 byte integer, nray x nscan); from the2AKu Radar Algorithm (PRE Module).

heightStormTop
altitude of storm top in Ku ray (4 byte float, nray x nscan); from the 2AKu Radar Algorithm (PRE Module).

binClutterFreeBottom
range bin of the lowest clutter-free bin of Ku ray (2 byte integer, nray x nscan); from the 2AKu Radar Algorithm (PRE Module).

sigmaZeroMeasured
measured surface normalized radar backscattering cross-section at Ku (4 byte float, nray x nscan); from the 2AKu Radar Algorithm (PRE Module).

zFactorMeasured
measured reflectivity at Ku (2 byte integer, nbin x nray x nscan); from the 2AKu Radar Algorithm (PRE Module).

ellipsoidBinOffset
offset along Ku ray between earth ellipsoid and midpoint of surface range bin (4 byte float, nray x nscan); from the 2AKu Radar Algorithm (PRE Module).

binZeroDeg
range bin of the zero degree isotherm in Ku ray (2 byte integer, nray x nscan); from the 2AKu Radar Algorithm (VER Module).

heightZeroDeg
altitude of the zero degree isotherm in Ku ray (4 byte float, nray x nscan); from the 2AKu Radar Algorithm (VER Module).

flagBB
flag indicating the detection of a bright-band in Ku ray (4 byte integer, nray x nscan); from the 2AKu Radar Algorithm (CSF Module).

binBBPeak
range bin of the bright-band maximum reflectivity, if detected, in Ku ray (2 byte integer, nray x nscan); from the 2AKu Radar Algorithm (CSF

Module).

heightBB
altitude of the bright-band maximum reflectivity, if detected, in Ku ray (4 byte float, nray x nscan); from the 2AKu Radar Algorithm (CSF Module).

qualityBB
quality flag for bright band detection in Ku ray (4 byte integer, nray x nscan); from the 2AKu Radar Algorithm (CSF Module).

type_Precip
classification of precipitation type in Ku ray (4 byte integer, nray x nscan); from the 2AKu Radar Algorithm (CSF Module).

qualityTypePrecip
quality of classification of precipitation type in Ku ray (4 byte integer, nray x nscan); from the 2AKu Radar Algorithm (CSF Module).

PIAalt
total 2-way path-integrated attenuation to the surface based upon surface reference technique methods for Ku (4 byte float, method x nray x nscan); from the 2AKu Radar Algorithm (SRT Module).

RFactorAlt
reliability factors of total 2-way path-integrated attenuation estimates based upon surface reference technique methods for Ku (4 byte float, method x nray x nscan); from the 2AKu Radar Algorithm (SRT Module).

PIAweight
weights of individual 2-way total path-integrated attenuation estimates to form effective estimate for Ku (4 byte float, method x nray x nscan); from the 2AKu Radar Algorithm (SRT Module).

pathAtten
effective total 2-way path-integrated attenuation to the surface based upon weighted averages of surface reference technique methods for Ku (4 byte float, nray x nscan); from the 2AKu Radar Algorithm (SRT Module).

reliabFactor
reliability factor of effective total 2-way path-integrated attenuation estimate based upon surface reference technique methods for Ku (4 byte float, nray x nscan); from the 2AKu Radar Algorithm (SRT Module).

reliabFlag
reliability flag for composite total 2-way path-integrated attenuation

estimate based upon surface reference methods for Ku (2 byte integer, nray x nscan); from the 2AKu Radar Algorithm (SRT Module).

phase

particle phase based on Ku (1 byte integer, nbin x nray x nscan); from the 2AKu Radar Algorithm (DSD Module).

binNode

bin node for partitioning radar profile based on Ku (4 byte integer, nNode x nray x nscan); from the 2AKu Radar Algorithm (DSD Module).

flagParticle

particle flag based on Ku (1 byte integer, nbin x nray x nscan); from the 2AKu Radar Algorithm (DSD Module).

from the 2AKuENV Radar Algorithm

airTemperature

air temperature interpolated to Ku range bins (4 byte float, nbin x nray x nscan); from JMA data using the 2AKuENV Radar Algorithm (VER Module).

airPressure

air pressure interpolated to Ku range bins (4 byte float, nbin x nray x nscan); from JMA data using the 2AKuENV Radar Algorithm (VER Module).

waterVapor

water vapor density interpolated to Ku range bins (4 byte float, nwater x nray x nscan); from JMA data using the 2AKuENV Radar Algorithm (VER Module).

cloudLiquidWater

cloud liquid water content interpolated to Ku range bins (4 byte float, nwater x nray x nscan); from JMA data using the 2AKuENV Radar Algorithm (VER Module).

surfacePressure

surface air pressure interpolated to Ku footprint location (4 byte float, nray x nscan); from JMA data using the 2AKuENV Radar Algorithm (VER Module).

groundTemperature

surface skin temperature interpolated to Ku footprint location (4 byte float, nray x nscan); from JMA data using the 2AKuENV Radar Algorithm (VER Module).

surfaceWind

10-meter wind speed interpolated to Ku footprint location (4 byte float, nwind x nray x nscan); from JMA analysis using the 2AKuENV Radar Algorithm (VER Module).

from the 2ADPR Radar Algorithm (NS)

Year

year of the Ku scan (2 byte integer, nscan); from the 2ADPR Radar Algorithm (in NS).

Month

month of the Ku scan (1 byte integer, nscan); from the 2ADPR Radar Algorithm (in NS).

DayOfMonth

day of month of the Ku scan (1 byte integer, nscan); from the 2ADPR Radar Algorithm (in NS).

Hour

hour of the Ku scan (1 byte integer, nscan); from the 2ADPR Radar Algorithm (in NS).

Minute

minute of the Ku scan (1 byte integer, nscan); from the 2ADPR Radar Algorithm (in NS).

Second

second of the Ku scan (1 byte integer, nscan); from the 2ADPR Radar Algorithm (in NS).

MilliSecond

millisecond of the Ku scan (2 byte integer, nscan); from the 2ADPR Radar Algorithm (in NS).

DayOfYear

day of the year of the Ku scan (2 byte integer, nscan); from the 2ADPR Radar Algorithm (in NS).

SecondOfDay

second of the day of the Ku scan (8 byte float, nscan); from the 2ADPR Radar Algorithm (in NS).

Latitude

latitude of Ku footprint (4 byte float, nray x nscan); from the 2ADPR Radar Algorithm (in NS).

Longitude

longitude of Ku footprint (4 byte float, nray x nscan); from the 2ADPR Radar Algorithm (in NS).

elevation

altitude above the Earth ellipsoid of the surface gate in Ku ray (4 byte float, nray x nscan); from the 2ADPR Radar Algorithm (PRE Module in NS).

landSurfaceType

water/land/coast and surface type at Ku footprint location (4 byte integer, nray x nscan); from the 2ADPR Radar Algorithm (PRE Module in NS). Note that this information is used to interpret surface reference technique output.

localZenithAngle

local incidence angles of DPR ray relative to local zenith on the Earth ellipsoid (4 byte float, nray x nscan); from the 2ADPR Radar Algorithm (PRE Module in NS).

flagPrecip

flag indicating detection of precipitation or no precipitation in Ku ray (4 byte integer, nray x nscan); from the 2ADPR Radar Algorithm (PRE Module in NS).

binRealSurface

surface range bin in Ku ray (2 byte integer, nray x nscan); from the 2ADPR Radar Algorithm (PRE Module in NS).

binStormTop

range bin of storm top in Ku ray (2 byte integer, nray x nscan); from the 2ADPR Radar Algorithm (PRE Module in NS).

heightStormTop

altitude of storm top in Ku ray (4 byte float, nray x nscan); from the 2ADPR Radar Algorithm (PRE Module in NS).

binClutterFreeBottom

range bin of the lowest clutter-free bin of Ku ray (2 byte integer, nray x nscan); from the 2ADPR Radar Algorithm (PRE Module in NS).

sigmaZeroMeasured

measured surface normalized radar backscattering cross-section at Ku (4 byte float, nray x nscan); from the 2ADPR Radar Algorithm (PRE Module in NS).

zFactorMeasured

measured reflectivity at Ku (2 byte integer, nbin x nray x nscan); from the 2ADPR Radar Algorithm (PRE Module in NS).

ellipsoidBinOffset
offset along Ku ray between earth ellipsoid and midpoint of surface range bin (4 byte float, nray x nscan); from the 2ADPR Radar Algorithm (PRE Module in NS).

binZeroDeg
range bin of the zero degree isotherm in Ku ray (2 byte integer, nray x nscan); from the 2ADPR Radar Algorithm (VER Module in NS).

heightZeroDeg
altitude of the zero degree isotherm in Ku ray (4 byte float, nray x nscan); from the 2ADPR Radar Algorithm (VER Module in NS).

flagBB
flag indicating the detection of a bright-band in Ku ray (4 byte integer, nray x nscan); from the 2ADPR Radar Algorithm (CSF Module in NS).

binBBPeak
range bin of the bright-band maximum reflectivity, if detected, in Ku ray (2 byte integer, nray x nscan); from the 2ADPR Radar Algorithm (CSF Module in NS).

heightBB
altitude of the bright-band maximum reflectivity, if detected, in Ku ray (4 byte float, nray x nscan); from the 2ADPR Radar Algorithm (CSF Module in NS).

qualityBB
quality flag for bright band detection in Ku ray (4 byte integer, nray x nscan); from the 2ADPR Radar Algorithm (CSF Module in NS).

type_Precip
classification of precipitation type in Ku ray (4 byte integer, nray x nscan); from the 2ADPR Radar Algorithm (CSF Module in NS).

qualityTypePrecip
quality of classification of precipitation type in Ku ray (4 byte integer, nray x nscan); from the 2ADPR Radar Algorithm (CSF Module in NS).

PIAalt
total 2-way path-integrated attenuation to the surface based upon surface reference technique methods for Ku (4 byte float, method x nray x nscan); from the 2ADPR Radar Algorithm (SRT Module in NS).

RFactorAlt

reliability factors of total 2-way path-integrated attenuation estimates based upon surface reference technique methods for Ku (4 byte float, method x nray x nscan); from the 2ADPR Radar Algorithm (SRT Module in NS).

PIAweight

weights of individual 2-way total path-integrated attenuation estimates to form effective estimate for Ku (4 byte float, method x nray x nscan); from the 2ADPR Radar Algorithm (SRT Module in NS).

pathAtten

effective total 2-way path-integrated attenuation to the surface based upon weighted averages of surface reference technique estimates for Ku (4 byte float, nray x nscan); from the 2ADPR Radar Algorithm (SRT Module in NS).

reliabFactor

reliability factor of effective total 2-way path-integrated attenuation estimate based upon surface reference technique methods for Ku (4 byte float, nray x nscan); from the 2ADPR Radar Algorithm (SRT Module in NS).

reliabFlag

reliability flag for effective total 2-way path-integrated attenuation estimate based upon surface reference methods for Ku (2 byte integer, nray x nscan); from the 2ADPR Radar Algorithm (SRT Module in NS).

phase

particle phase based on Ku (1 byte integer, nbin x nray x nscan); from the 2ADPR Radar Algorithm (DSD Module in NS).

binNode

bin node for partitioning radar profile based on Ku (4 byte integer, nNode x nray x nscan); from the 2ADPR Radar Algorithm (DSD Module in NS).

flagParticle

particle flag based on Ku (1 byte integer, nbin x nray x nscan); from the 2ADPR Radar Algorithm (DSD Module in NS).

from the 2ADPR Radar Algorithm (MS)

Year

year of the Ka scan (2 byte integer, nscan); from the 2ADPR Radar Algorithm (in MS).

Month

month of the Ka scan (1 byte integer, nscan); from the 2ADPR Radar Algorithm (in MS).

DayOfMonth

day of month of the Ka scan (1 byte integer, nscan); from the 2ADPR Radar Algorithm (in MS).

Hour

hour of the Ka scan (1 byte integer, nscan); from the 2ADPR Radar Algorithm (in MS).

Minute

minute of the Ka scan (1 byte integer, nscan); from the 2ADPR Radar Algorithm (in MS).

Second

second of the Ka scan (1 byte integer, nscan); from the 2ADPR Radar Algorithm (in MS).

MilliSecond

millisecond of the Ka scan (2 byte integer, nscan); from the 2ADPR Radar Algorithm (in MS).

DayOfYear

day of the year of the Ka scan (2 byte integer, nscan); from the 2ADPR Radar Algorithm (in MS).

SecondOfDay

second of the day of the Ka scan (8 byte float, nscan); from the 2ADPR Radar Algorithm (in MS).

Latitude

latitude of Ka footprint (4 byte float, nrayMS x nscan); from the 2ADPR Radar Algorithm (in MS).

Longitude

longitude of Ka footprint (4 byte float, nrayMS x nscan); from the 2ADPR Radar Algorithm (in MS).

elevation

altitude above the Earth ellipsoid of the surface gate in Ka ray (4 byte float, nrayMS x nscan); from the 2ADPR Radar Algorithm (PRE Module in MS).

landSurfaceType

water/land/coast and surface type at Ka footprint location (4 byte integer, nrayMS x nscan); from the 2ADPR Radar Algorithm (PRE Module in MS). Note that this information is used to interpret surface reference technique output.

localZenithAngle

local incidence angles of DPR ray relative to local zenith on the Earth ellipsoid (4 byte float, nrayMS x nscan); from the 2ADPR Radar Algorithm (PRE Module in MS).

flagPrecip

flag indicating detection of precipitation or no precipitation in Ka ray (4 byte integer, nrayMS x nscan); from the 2ADPR Radar Algorithm (PRE Module in MS).

binRealSurface

surface range bin in Ka ray (2 byte integer, nrayMS x nscan); from the 2ADPR Radar Algorithm (PRE Module in MS).

binStormTop

range bin of storm top in Ka ray (2 byte integer, nrayMS x nscan); from the 2ADPR Radar Algorithm (PRE Module in MS).

heightStormTop

altitude of storm top in Ka ray (4 byte float, nrayMS x nscan); from the 2ADPR Radar Algorithm (PRE Module in MS).

binClutterFreeBottom

range bin of the lowest clutter-free bin of Ka ray (2 byte integer, nrayMS x nscan); from the 2ADPR Radar Algorithm (PRE Module in MS).

sigmaZeroMeasured

measured surface normalized radar backscattering cross-section at Ka (4 byte float, nrayMS x nscan); from the 2ADPR Radar Algorithm (PRE Module in MS).

zFactorMeasured

measured reflectivity at Ka (2 byte integer, nbin x nrayMS x nscan); from the 2ADPR Radar Algorithm (PRE Module in MS).

ellipsoidBinOffset

offset along Ka ray between earth ellipsoid and midpoint of surface range bin (4 byte float, nrayMS x nscan); from the 2ADPR Radar Algorithm (PRE Module in MS).

binZeroDeg

range bin of the zero degree isotherm in Ka ray (2 byte integer, nrayMS x nscan); from the 2ADPR Radar Algorithm (VER Module in MS).

heightZeroDeg
altitude of the zero degree isotherm in Ka ray (4 byte float, nrayMS x nscan); from the 2ADPR Radar Algorithm (VER Module in MS).

flagBB
flag indicating the detection of a bright-band in Ka ray (4 byte integer, nrayMS x nscan); from the 2ADPR Radar Algorithm (CSF Module in MS).

binBBPeak
range bin of the bright-band maximum reflectivity, if detected, in Ka ray (2 byte integer, nrayMS x nscan); from the 2ADPR Radar Algorithm (CSF Module in MS).

heightBB
altitude of the bright-band maximum reflectivity, if detected, in Ka ray (4 byte float, nrayMS x nscan); from the 2ADPR Radar Algorithm (CSF Module in MS).

qualityBB
quality flag for bright band detection in Ka ray (4 byte integer, nrayMS x nscan); from the 2ADPR Radar Algorithm (CSF Module in MS).

type_Precip
classification of precipitation type in Ka ray (4 byte integer, nrayMS x nscan); from the 2ADPR Radar Algorithm (CSF Module in MS).

qualityTypePrecip
quality of classification of precipitation type in Ka ray (4 byte integer, nrayMS x nscan); from the 2ADPR Radar Algorithm (CSF Module in MS).

PIAalt
total 2-way path-integrated attenuation to the surface based upon surface reference technique methods for Ka (4 byte float, method x nrayMS x nscan); from the 2ADPR Radar Algorithm (SRT Module in MS).

RFactorAlt
reliability factors of total 2-way path-integrated attenuation estimates based upon surface reference technique methods for Ka (4 byte float, method x nrayMS x nscan); from the 2ADPR Radar Algorithm (SRT Module in MS).

PIAweight
weights of individual 2-way total path-integrated attenuation estimates

to form effective estimates for Ka (4 byte float, method x nrayMS x nscan); from the 2ADPR Radar Algorithm (SRT Module in MS).

pathAtten

effective total 2-way path-integrated attenuation to the surface based upon weighted averages of surface reference technique estimates for Ka (4 byte float, nrayMS x nscan); from the 2ADPR Radar Algorithm (SRT Module in MS).

reliabFactor

reliability factor of effective total 2-way path-integrated attenuation estimate based upon surface reference technique methods for Ka (4 byte float, nrayMS x nscan); from the 2ADPR Radar Algorithm (SRT Module in MS).

reliabFlag

reliability flag for composite total 2-way path-integrated attenuation estimate based upon surface reference methods for Ka (2 byte integer, nrayMS x nscan); from the 2ADPR Radar Algorithm (SRT Module in MS).

phase

particle phase based on Ka (1 byte integer, nbin x nrayMS x nscan); from the 2ADPR Radar Algorithm (DSD Module in MS).

binNode

bin node for partitioning radar profile based on Ka (4 byte integer, nNode x nrayMS x nscan); from the 2ADPR Radar Algorithm (DSD Module in MS).

flagParticle

particle flag based on Ka (1 byte integer, nbin x nrayMS x nscan); from the 2ADPR Radar Algorithm (DSD Module in MS).

<u>from the 1CGMI Algorithm (S1)</u>

Year

year of the GMI scan (2 byte integer, nscan1) from the 1CGMI Algorithm (in S1).

Month

month of the GMI scan (1 byte integer, nscan1) from the 1CGMI Algorithm (in S1).

DayOfMonth

day of month of the GMI scan (1 byte integer, nscan1) from the 1CGMI

Algorithm (in S1).

Hour

hour of the GMI scan (1 byte integer, nscan1) from the 1CGMI Algorithm (in S1).

Minute

minute of the GMI scan (1 byte integer, nscan1) from the 1CGMI Algorithm (in S1).

Second

second of the GMI scan (1 byte integer, nscan1) from the 1CGMI Algorithm (in S1).

MilliSecond

millisecond of the GMI scan (2 byte integer, nscan1) from the 1CGMI Algorithm (in S1).

DayOfYear

day of year of the GMI scan (2 byte integer, nscan1); from the 1CGMI Algorithm (in S1).

SecondOfDay

second of day of the GMI scan (8 byte float, nscan1); from the 1CGMI Algorithm (in S1).

Latitude

latitude of the GMI footprint (4 byte float, npixel1 x nscan1); from the 1CGMI Algorithm (in S1).

Longitude

longitude of the GMI footprint (4 byte float, npixel1 x nscan1); from the 1CGMI Algorithm (in S1).

Quality

quality of the lower-frequency calibrated brightness temperatures (1 byte integer, npixel1 x nscan1); from the 1CGMI Algorithm (in S1).

incidenceAngle

earth incidence angle of the GMI lower-frequency data (4 byte float, nchUIA1 x npixel1 x nscan1); from the 1CGMI Algorithm (in S1).

sunGlintAngle

sun glint angles of the GMI lower-frequency data (1 byte integer, nchUIA1 x npixel1 x nscan1); from the 1CGMI Algorithm (in S1).

incidenceAngleIndex

index of the incidence angle array for each lower-frequency channel (1 byte integer, nchannel1 x nscan1); from the 1CGMI Algorithm (in S1).

Tc

common calibrated GMI brightness temperatures in the lower-frequency data swath (4 byte float, nchannel1 x npixel1 x nscan1); from the 1CGMI Algorithm (in S1).

from the 1CGMI Algorithm (S2)

Year

year of the GMI scan (2 byte integer, nscan2) from the 1CGMI Algorithm (in S2).

Month

month of the GMI scan (1 byte integer, nscan2) from the 1CGMI Algorithm (in S2).

DayOfMonth

day of month of the GMI scan (1 byte integer, nscan2) from the 1CGMI Algorithm (in S2).

Hour

hour of the GMI scan (1 byte integer, nscan2) from the 1CGMI Algorithm (in S2).

Minute

minute of the GMI scan (1 byte integer, nscan2) from the 1CGMI Algorithm (in S2).

Second

second of the GMI scan (1 byte integer, nscan2) from the 1CGMI Algorithm (in S2).

MilliSecond

millisecond of the GMI scan (2 byte integer, nscan2) from the 1CGMI Algorithm (in S2).

DayOfYear

day of year of the GMI scan (2 byte integer, nscan2); from the 1CGMI Algorithm (in S2).

SecondOfDay

second of day of the GMI scan (8 byte float, nscan2); from the 1CGMI Algorithm (in S2).

Latitude

latitude of the GMI footprint (4 byte float, npixel2 x nscan2); from the 1CGMI Algorithm (in S2).

Longitude

longitude of the GMI footprint (4 byte float, npixel2 x nscan2); from the 1CGMI Algorithm (in S2).

Quality

quality of the higher-frequency calibrated brightness temperatures (1 byte integer, npixel2 x nscan2); from the 1CGMI Algorithm (in S2).

incidenceAngle

earth incidence angles of the GMI higher-frequency data (4 byte float, nchUIA2 x npixel2 x nscan2); from the 1CGMI Algorithm (in S2).

sunGlintAngle

sun glint angles of the GMI higher-frequency data (1 byte integer, nchUIA2 x npixel2 x nscan2); from the 1CGMI Algorithm (in S2).

incidenceAngleIndex

index of the incidence angle array for each higher-frequency channel (1 byte integer, nchannel2 x nscan2); from the 1CGMI Algorithm (in S2).

Tc

common calibrated GMI brightness temperatures in the higher-frequency data swath (4 byte float, nchannel2 x npixel2 x nscan2); from the 1CGMI Algorithm (in S2).

Output Parameters
Note standard output products are sampled at 250 m vertical resolution. The given array size arguments correspond to:

nscan = number of DPR scans per granule, approximately 7900
nrayNS = 49 rays in each Ku band (NS) scan
nrayMS = 25 rays in each matched Ku-Ka (MS) scan
nbinC = 88 vertical range bins at 250 m intervals
nbinEnv = 10 range bins for environmental parameter sampling
nbinLow = 9 range bins for low-resolution PSD parameter sampling
nbinPhase = 5 range bins indicating phase transitions
nbinTrans = 10 range bins describing the precipitation liquid phase fraction through the mixed phase layer
nPSDhigh = 1 parameters for describing the precipitation particle size distribution at 250 m resolution
nPSDlow = 2 parameters for describing the precipitation particle size distribution at low vertical resolution.
nAB = 2 power law parameters to describe particle densities
nKuKa = 2 indices for the Ku and Ka channels
nchan = 15 GMI channels, including separate accounting for the double side-band channels.

<u>from the 2BCMB Combined Radar-Radiometer Algorithm (NS)</u>

Year
year of the Ku band scan (2 byte integer, nscan); from the 2BCMB Combined Algorithm (in NS/ScanTime).

Month
month of the Ku band scan (1 byte integer, nscan); from the 2BCMB Combined Algorithm (in NS/ScanTime).

DayOfMonth
day of month of the Ku band scan (1 byte integer, nscan); from the 2BCMB Combined Algorithm (in NS/ScanTime).

Hour
hour of the Ku band scan (1 byte integer, nscan); from the 2BCMB Combined Algorithm (in NS/ScanTime).

Minute
minute of the Ku band scan (1 byte integer, nscan); from the 2BCMB Combined Algorithm (in NS/ScanTime).

Second
second of the Ku band scan (1 byte integer, nscan); from the 2BCMB

Combined Algorithm (in NS/ScanTime).

MilliSecond

millisecond of the Ku band scan (2 byte integer, nscan); from the 2BCMB Combined Algorithm (in NS/Scantime).

DayOfYear

day of year of the Ku band scan (2 byte integer, nscan); from the 2BCMB Combined Algorithm (in NS/ScanTime).

SecondOfDay

second of day of the Ku band scan (8 byte float, nscan); from the 2BCMB Combined Algorithm (in NS/ScanTime).

Latitude

latitude of Ku band footprint (4 byte float, nrayNS x nscan); from the 2BCMB Combined Algorithm (in NS).

Longitude

longitude of Ku band footprint (4 byte float, nrayNS x nscan); from the 2BCMB Combined Algorithm (in NS).

ioQuality

6-digit flag describing the quality of input data and precipitation estimate (4 byte integer, nrayNS x nscan); from the 2BCMB Combined Algorithm (in NS/FLG).

1's digit:	0 if estimate is valid
	9 if no estimate
10's digit:	0 if Ku data valid and rain detected at Ku
	1 if Ku data valid but no rain detected
	9 if bad Ku input data
100's digit:	0 if Ku SRT gives viable PIA estimate
	1 if σ^o_{Ku} is within noise of background
	2 if σ^o_{Ku} is completely attenuated
	9 if bad Ku input data
1000s digit:	0 if freezing level derived from Ku bright band
	1 if freezing level derived from meteorological analysis
	9 if bad Ku input data
10000's digit:	0 if Ku classified as stratiform or convective
	1 if Ku classified as indeterminate
	2 if precip not detected at Ku (no feature)
	9 if bad Ku input data
100000's digit:	0 if at least some measured brightness temperatures are valid

9 if no measured brightness temperatures are valid

multiScatCalc

flag indicating whether or not multiple-scattering radar calculations are utilized at Ka band (1) or not (0), or that no rain was detected -9999. Although output in NS mode, this variable is only applicable to MS mode, and so a flag value is output in NS model (in NS/FLG).

surfaceElevation

altitude above the Earth ellipsoid of the surface gate in Ku band ray (4 byte float, nrayNS x nscan); from the 2BCMB Combined Algorithm (in NS/Input).

surfaceType

water/land/coast and surface type at Ku band footprint location (4 byte integer, nrayNS x nscan); from the 2BCMB Combined Algorithm (in NS/Input).

localZenithAngle

local incidence angle of Ku band ray relative to local zenith on the Earth ellipsoid (4 byte float, nrayNS x nscan); from the 2BCMB Combined Algorithm (in NS/Input).

precipitationFlag

flag indicating detection of precipitation or no precipitation in Ku band ray (4 byte integer, nrayNS x nscan); from the 2BCMB Combined Algorithm (in NS/Input).

surfaceRangeBin

surface range bin in Ku band ray (2 byte integer, nrayNS x nscan); from the 2BCMB Combined Algorithm (in NS/Input).

lowestClutterFreeBin

lowest clutter free bin in Ku band ray (2 byte integer, nrayNS x nscan); from the 2BCMB Combined Algorithm (in NS/Input).

ellipsoidBinOffset

offset along Ku ray between earth ellipsoid and midpoint of surface range bin (4 byte float, nrayNS x nscan); from the 2BCMB Combined Algorithm (in NS/Input).

stormTopBin

storm top range bin in Ku band ray (2 byte integer, nrayNS x nscan); from the 2BCMB Combined Algorithm (in NS/Input).

stormTopAltitude

storm top altitude in Ku band ray (4 byte float, nrayNS x nscan); from the 2BCMB Combined Algorithm (in NS/Input).

zeroDegBin

freezing level bin in Ku band ray (2 byte integer, nrayNS x nscan); from the 2BCMB Combined Algorithm (in NS/Input).

zeroDegAltitude

freezing level altitude in Ku band ray (4 byte float, nrayNS x nscan); from the 2BCMB Combined Algorithm (in NS/Input).

precipitationType

classification of precipitation type in Ku band ray (4 byte integer, nrayNS x nscan); from the 2BCMB Combined Algorithm (in NS/Input).

precipTypeQualityFlag

quality of classification of precipitation type in Ku band ray (4 byte integer, nrayNS x nscan); from the 2BCMB Combined Algorithm (in NS/Input).

piaEffective

effective total 2-way path-integrated attenuation to the surface at Ku band, based upon weighted averages of surface reference technique estimates (4 byte float, nrayNS x nscan); from the 2BCMB Combined Algorithm (in NS/Input).

piaEffectiveSigma

uncertainty of effective total 2-way path-integrated attenuation at Ku band based upon surface reference technique methods (4 byte float, nrayNS x nscan); from the 2BCMB Combined Algorithm (in NS/Input).

piaEffectiveReliabFlag

reliability flag of the effective total 2-way path-integrated attenuation at Ku band, based upon weighted averages of surface reference technique estimates (2 byte integer, nrayNS x nscan); from the 2BCMB Combined Algorithm (in NS/Input).

snowIceCover

flag indicating the presence (2) or absence (1) of snow on the earth's surface (4-byte integer, nrayNS x nscan). Ocean is indicated by 0. (in NS/Input)

surfaceAirPressure

surface air pressure at the Ku band footprint location (4 byte float, nrayNS x nscan); from the 2BCMB Combined Algorithm (in NS).

surfaceAirTemperature

surface air temperature at the Ku band footprint location (4 byte float, nrayNS x nscan); from the 2BCMB Combined Algorithm (in NS).

surfaceVaporDensity

surface vapor density at the Ku band footprint location (4 byte float, nrayNS x nscan); from the 2BCMB Combined Algorithm (in NS).

skinTemperature

surface skin temperature at the Ku band footprint location (4 byte float, nrayNS x nscan); from the 2BCMB Combined Algorithm (in NS).

envParamNode

bin numbers where environmental pressure, temperature, and vapor density are sampled (2 byte integer, nbinEnv x nrayNS x nscan) from 2BCMB Combined Algorithm (in NS).

airPressure

air pressure along the Ku band ray at the envParamNode locations (4 byte float, nbinEnv x nrayNS x nscan); from the 2BCMB Combined Algorithm (in NS).

airTemperature

air temperature along the Ku band ray at the envParamNode locations (4 byte float, nbinEnv x nrayNS x nscan); from the 2BCMB Combined Algorithm (in NS).

vaporDensity

vapor density along the Ku band ray at the envParamNode locations (4 byte integer, nbinEnv x nrayNS x nscan); from the 2BCMB Combined Algorithm (in NS).

cloudLiqWaterCont

cloud liquid water content along the Ku band ray at 250 m sampling resolution (4 byte float, nbinC x nrayNS x nscan); from the 2BCMB Combined Algorithm (in NS).

cloudIceWaterCont

cloud ice liquid-equivalent water content along the Ku band ray at 250 m sampling resolution (4 byte float, nbinC x nrayNS x nscan); from the 2BCMB Combined Algorithm (in NS). Currently this parameter is not assigned.

phaseBinNodes

bin numbers indicating (0) storm top, (1) top of mixed-phase layer, (2) maximum reflectivity in mixed-phase layer if bright band detected;

otherwise, the freezing level from analysis, (3) bottom of mixed-phase layer, and (4) bottom of rain layer (2 byte integer, nbinPhase x nrayNS x nscan); from 2BCMB Combined Algorithm (in NS).

liqMassFracTrans

fraction of the precipitation mass that is liquid in the transition between ice and liquid-phase precipitation, starting from the top of the mixed-phase layer (phaseBinNode 1) and proceeding downward along the Ku band ray at 250 m sampling resolution (4 byte float, nbinTrans x nrayNS x nscan); from the 2BCMB Combined Algorithm (in NS).

liqRateFracTrans

fraction of the precipitation rate that is liquid in the transition between ice and liquid-phase precipitation, starting from the top of the mixed-phase layer (phaseBinNode 1) and proceeding downward along the Ku band ray at 250 m sampling resolution (4 byte float, nbinTrans x nrayNS x nscan); from the 2BCMB Combined Algorithm (in NS).

precipTotRate

precipitation rate along the Ku band ray at 250 m sampling resolution (4 byte float, nbinC x nrayNS x nscan); from the 2BCMB Combined Algorithm (in NS).

precipTotRateSigma

uncertainty of precipitation rate along the Ku band ray at 250 m sampling resolution (4 byte float, nbinC x nrayNS x nscan); from the 2BCMB Combined Algorithm (in NS).

precipTotWaterCont

precipitation water content along the Ku band ray at 250 m sampling resolution (4 byte float, nbinC x nrayNS x nscan); from the 2BCMB Combined Algorithm (in NS).

precipTotWaterContSigma

uncertainty of precipitation water content along the Ku band ray at 250 m sampling resolution (4 byte float, nbinC x nrayNS x nscan); from the 2BCMB Combined Algorithm (in NS).

precipTotPSDparamHigh

precipitation drop-size distribution mean volume diameter (D_m) along the Ku band ray at 250 m sampling resolution (4 byte float, nPSDhigh x nbinC x nrayNS x nscan); from the 2BCMB Combined Algorithm (in NS).

PSDparamLowNode

bin numbers where low-resolution precipitation PSD parameters are sampled (2 byte integer, nbinLow x nrayNS x nscan) from 2BCMB

Combined Algorithm (in NS).

precipTotPSDparamLow

precipitation drop-size distribution parameters ($\log(N_w)$, μ) along the Ku band ray at reduced sampling resolution (2 byte integer, nPSDlow x nbinLow x nrayNS x nscan); from the 2BCMB Combined Algorithm (in NS).

surfPrecipTotRate

surface precipitation rate at Ku footprint location (4 byte float, nrayNS x nscan); from the 2BCMB Combined Algorithm (in NS).

surfPrecipTotRateSigma

surface precipitation rate uncertainty at Ku footprint location (4 byte float, nrayNS x nscan); from the 2BCMB Combined Algorithm (in NS).

surfLiqRateFrac

fraction of the surface precipitation rate that is liquid at the Ku footprint location (4 byte float, nrayNS x nscan); from the 2BCMB Combined Algorithm (in NS).

tenMeterWindSpeed

10-meter wind speed at Ku footprint location (4 byte float, nrayNS x nscan); from the 2BCMB Combined Algorithm (in NS).

tenMeterWindSigma

estimated uncertainty of 10-meter wind speed at Ku footprint location (4 byte float, nrayNS x nscan); from the 2BCMB Combined Algorithm. Estimates are for water surfaces only (in NS).

surfEmissivity

microwave surface emissivities at the GMI channel frequencies/polarizations and viewing angle at Ku footprint location (4 byte float, nchan x nrayNS x nscan); from the 2BCMB Combined Algorithm (in NS).

surfEmissSigma

estimated uncertainties of microwave surface emissivities at the GMI channel frequencies/polarizations and viewing angle at Ku footprint location (4 byte float, nchan x nrayNS x nscan); from the 2BCMB Combined Algorithm. Estimates over land, only (in NS).

simulatedBrightTemp

upwelling microwave surface brightness temperatures at the GMI channel frequencies/polarizations and viewing angle (4 byte float, nchan x nrayNS x nscan); from the 2BCMB Combined Algorithm (in NS).

pia

total path-integrated attenuation at Ku (4 byte float, nrayNS x nscan); from the 2BCMB Combined Algorithm (in NS).

correctedReflectFactor

attenuation-corrected radar reflectivity factor along Ku ray at 250 m sampling resolution (4 byte float, nbinC x nrayNS x nscan); from the 2BCMB Combined Algorithm.

multiScatMaxContrib

the maximum contribution by multiple scattering to a reflectivity simulation (4 byte float, nrayNS x nscan) in the given radar profile. Although output in NS, multiple-scattering is only calculated for simulated Ka band reflectivities, and so a flag value is output (in NS).

nubfPIAfactor

the fractional reduction of the Hitschfeld-Bordan estimated path-integrated attenuation for simulating the Surface Reference Technique path-integrated attenuation (4 byte float, nrayNS x nscan). Since the non-uniform beamfilling fraction is only calculated for Ka band, a flag value is output for this parameter (in NS).

from the 2BCMB Combined Radar-Radiometer Algorithm (MS)

Year

year of the Ka band scan (2 byte integer, nscan); from the 2BCMB Combined Algorithm (in MS/ScanTime).

Month

month of the Ka band scan (1 byte integer, nscan); from the 2BCMB Combined Algorithm (in MS/ScanTime).

DayOfMonth

day of month of the Ka band scan (1 byte integer, nscan); from the 2BCMB Combined Algorithm (in MS/ScanTime).

Hour

hour of the Ka band scan (1 byte integer, nscan); from the 2BCMB Combined Algorithm (in MS/ScanTime).

Minute

minute of the Ka band scan (1 byte integer, nscan); from the 2BCMB Combined Algorithm (in MS/ScanTime).

Second

second of the Ka band scan (1 byte integer, nscan); from the 2BCMB Combined Algorithm (in MS/ScanTime).

MilliSecond

millisecond of the Ka band scan (2 byte integer, nscan); from the 2BCMB Combined Algorithm (in MS/Scantime).

DayOfYear

day of year of the Ka band scan (2 byte integer, nscan); from the 2BCMB Combined Algorithm (in MS/ScanTime).

SecondOfDay

second of day of the Ka band scan (8 byte float, nscan); from the 2BCMB Combined Algorithm (in MS/ScanTime).

Latitude

latitude of Ka band footprint (4 byte float, nrayMS x nscan); from the 2BCMB Combined Algorithm (in MS).

Longitude

longitude of Ka band footprint (4 byte float, nrayMS x nscan); from the 2BCMB Combined Algorithm (in MS).

ioQuality

6-digit flag describing the quality of input data and precipitation estimate (4 byte integer, nrayMS x nscan); from the 2BCMB Combined Algorithm (in MS/FLG). Currently, this is just a replica of the NS mode ioQuality flag.

1's digit:	0 if estimate is valid
	9 if no estimate
10's digit:	0 if Ku data valid and rain detected at Ku
	1 if Ku data valid but no rain detected
	9 if bad Ku input data
100's digit:	0 if Ku SRT gives viable PIA estimate
	1 if σ^{o}_{Ku} is within noise of background
	2 if σ^{o}_{Ku} is completely attenuated
	9 if bad Ku input data
1000s digit:	0 if freezing level derived from Ku bright band
	1 if freezing level derived from meteorological analysis
	9 if bad Ku input data
10000's digit:	0 if Ku classified as stratiform or convective
	1 if Ku classified as indeterminate
	2 if precip not detected at Ku (no feature)
	9 if bad Ku input data
100000's digit:	0 if at least some measured brightness temperatures

are valid
9 if no measured brightness temperatures are valid

multiScatCalc
flag indicating whether or not multiple-scattering radar calculations are utilized at Ka band (1) or not (0), or that no rain was detected -9999 (4 byte integer, nrayMS x nscan). Location (in MS/FLG)

surfaceElevation
altitude above the Earth ellipsoid of the surface gate in Ka band ray (4 byte float, nrayMS x nscan); from the 2BCMB Combined Algorithm (in MS/Input).

surfaceType
water/land/coast and surface type at Ka band footprint location (4 byte integer, nrayMS x nscan); from the 2BCMB Combined Algorithm (in MS/Input).

localZenithAngle
local incidence angle of Ka band ray relative to local zenith on the Earth ellipsoid (4 byte float, nrayMS x nscan); from the 2BCMB Combined Algorithm (in MS/Input).

precipitationFlag
flag indicating detection of precipitation or no precipitation in Ka band ray (4 byte integer, nrayMS x nscan); from the 2BCMB Combined Algorithm (in MS/Input).

surfaceRangeBin
surface range bin in Ka band ray (2 byte integer, nrayMS x nscan); from the 2BCMB Combined Algorithm (in MS/Input).

lowestClutterFreeBin
lowest clutter free bin in Ka band ray (2 byte integer, nrayMS x nscan); from the 2BCMB Combined Algorithm (in MS/Input).

ellipsoidBinOffset
offset along Ka ray between earth ellipsoid and midpoint of surface range bin (4 byte float, nrayMS x nscan); from the 2BCMB Combined Algorithm (in MS/Input).

stormTopBin
storm top range bin in Ka band ray (2 byte integer, nrayMS x nscan); from the 2BCMB Combined Algorithm (in MS/Input).

stormTopAltitude

storm top altitude in Ka band ray (4 byte float, nrayMS x nscan); from the 2BCMB Combined Algorithm (in MS/Input).

zeroDegBin
freezing level bin in Ka band ray (2 byte integer, nrayMS x nscan); from the 2BCMB Combined Algorithm (in MS/Input).

zeroDegAltitude
freezing level altitude in Ka band ray (4 byte float, nrayMS x nscan); from the 2BCMB Combined Algorithm (in MS/Input).

precipitationType
classification of precipitation type in Ka band ray (4 byte integer, nrayMS x nscan); from the 2BCMB Combined Algorithm (in MS/Input).

precipTypeQualityFlag
quality of classification of precipitation type in Ka band ray (4 byte integer, nrayMS x nscan); from the 2BCMB Combined Algorithm (in MS/Input).

piaEffective
effective total 2-way path-integrated attenuation to the surface at Ku and Ka bands, based upon weighted averages of surface reference technique estimates (4 byte float, nKuKa x nrayMS x nscan); from the 2BCMB Combined Algorithm (in MS/Input).

piaEffectiveSigma
uncertainty of effective total 2-way path-integrated attenuation at Ku and Ka bands based upon surface reference technique methods (4 byte float, nKuKa x nrayMS x nscan); from the 2BCMB Combined Algorithm (in MS/Input).

piaEffectiveReliabFlag
reliability flag of the effective total 2-way path-integrated attenuation at Ku and Ka bands, based upon weighted averages of surface reference technique estimates (2 byte integer, nKuKa x nrayMS x nscan); from the 2BCMB Combined Algorithm (in MS/Input).

snowIceCover
flag indicating the presence (2) or absence (1) of snow on the earth's surface (4-byte integer, nrayMS x nscan). Ocean is indicated by 0. (in MS/Input)

surfaceAirPressure
surface air pressure at the Ka band footprint location (4 byte float, nrayMS x nscan); from the 2BCMB Combined Algorithm (in MS).

surfaceAirTemperature
surface air temperature at the Ka band footprint location (4 byte float, nrayMS x nscan); from the 2BCMB Combined Algorithm (in MS).

surfaceVaporDensity
surface vapor density at the Ka band footprint location (4 byte float, nrayMS x nscan); from the 2BCMB Combined Algorithm (in MS).

skinTemperature
surface skin temperature at the Ka band footprint location (4 byte float, nrayMS x nscan); from the 2BCMB Combined Algorithm (in MS).

envParamNode
bin numbers where environmental pressure, temperature, and vapor density are sampled (2 byte integer, nbinEnv x nrayMS x nscan) from 2BCMB Combined Algorithm (in MS).

airPressure
air pressure along the Ka band ray at the envParamNode locations (4 byte float, nbinEnv x nrayMS x nscan); from the 2BCMB Combined Algorithm (in MS).

airTemperature
air temperature along the Ka band ray at the envParamNode locations (4 byte float, nbinEnv x nrayMS x nscan); from the 2BCMB Combined Algorithm (in MS).

vaporDensity
vapor density along the Ka band ray at the envParamNode locations (4 byte integer, nbinEnv x nrayMS x nscan); from the 2BCMB Combined Algorithm (in MS).

cloudLiqWaterCont
cloud liquid water content along the Ka band ray at 250 m sampling resolution (4 byte float, nbinC x nrayMS x nscan); from the 2BCMB Combined Algorithm (in MS).

cloudIceWaterCont
cloud ice liquid-equivalent water content along the Ka band ray at 250 m sampling resolution (4 byte float, nbinC x nrayMS x nscan); from the 2BCMB Combined Algorithm (in MS). Currently this parameter is not assigned.

phaseBinNodes
bin numbers indicating (0) storm top, (1) top of mixed-phase layer, (2)

maximum reflectivity in mixed-phase layer if bright band detected; otherwise, the freezing level from analysis, (3) bottom of mixed-phase layer, and (4) bottom of rain layer (2 byte integer, nbinPhase x nrayMS x nscan); from 2BCMB Combined Algorithm (in MS).

liqMassFracTrans

fraction of the precipitation mass that is liquid in the transition between ice and liquid-phase precipitation, starting from the top of the mixed-phase layer (phaseBinNode 1) and proceeding downward along the Ka band ray at 250 m sampling resolution (4 byte float, nbinTrans x nrayMS x nscan); from the 2BCMB Combined Algorithm (in MS).

liqRateFracTrans

fraction of the precipitation rate that is liquid in the transition between ice and liquid-phase precipitation, starting from the top of the mixed-phase layer (phaseBinNode 1) and proceeding downward along the Ku band ray at 250 m sampling resolution (4 byte float, nbinTrans x nrayMS x nscan); from the 2BCMB Combined Algorithm (in MS).

precipTotRate

precipitation rate along the Ka band ray at 250 m sampling resolution (4 byte float, nbinC x nrayMS x nscan); from the 2BCMB Combined Algorithm (in MS).

precipTotRateSigma

uncertainty of precipitation rate along the Ka band ray at 250 m sampling resolution (4 byte float, nbinC x nrayMS x nscan); from the 2BCMB Combined Algorithm (in MS).

precipTotWaterCont

precipitation water content along the Ka band ray at 250 m sampling resolution (4 byte float, nbinC x nrayMS x nscan); from the 2BCMB Combined Algorithm (in MS).

precipTotWaterContSigma

uncertainty of precipitation water content along the Ka band ray at 250 m sampling resolution (4 byte float, nbinC x nrayMS x nscan); from the 2BCMB Combined Algorithm (in MS).

precipTotPSDparamHigh

precipitation drop-size distribution mean volume diameter (D_m) along the Ka band ray at 250 m sampling resolution (4 byte float, nPSDhigh x nbinC x nrayMS x nscan); from the 2BCMB Combined Algorithm (in MS).

PSDparamLowNode

bin numbers where low-resolution precipitation PSD parameters are

sampled (2 byte integer, nbinLow x nrayMS x nscan) from 2BCMB Combined Algorithm (in MS).

precipTotPSDparamLow
precipitation drop-size distribution parameters (log(Nw), μ) along the Ka band ray at reduced sampling resolution (2 byte integer, nPSDlow x nbinLow x nrayMS x nscan); from the 2BCMB Combined Algorithm (in MS).

surfPrecipTotRate
surface precipitation rate at Ka footprint location (4 byte float, nrayMS x nscan); from the 2BCMB Combined Algorithm (in MS).

surfPrecipTotRateSigma
surface precipitation rate uncertainty at Ka footprint location (4 byte float, nrayMS x nscan); from the 2BCMB Combined Algorithm (in MS).

surfLiqRateFrac
fraction of the surface precipitation rate that is liquid at the Ka footprint location (4 byte float, nrayMS x nscan); from the 2BCMB Combined Algorithm (in MS).

tenMeterWindSpeed
10-meter wind speed at Ka footprint location (4 byte float, nrayMS x nscan); from the 2BCMB Combined Algorithm (in MS).

tenMeterWindSigma
estimated uncertainty of 10-meter wind speed at Ka footprint location (4 byte float, nrayMS x nscan); from the 2BCMB Combined Algorithm. Estimates are for water surfaces only (in MS).

surfEmissivity
microwave surface emissivities at the GMI channel frequencies/polarizations and viewing angle at Ka footprint location (4 byte float, nchan x nrayMS x nscan); from the 2BCMB Combined Algorithm (in MS).

surfEmissSigma
estimated uncertainties of microwave surface emissivities at the GMI channel frequencies/polarizations and viewing angle at Ka footprint location (4 byte float, nchan x nrayMS x nscan); from the 2BCMB Combined Algorithm. Estimates over land, only (in MS).

simulatedBrightTemp
upwelling microwave surface brightness temperatures at the GMI channel frequencies/polarizations and viewing angle (4 byte float, nchan

x nrayMS x nscan); from the 2BCMB Combined Algorithm (in MS).

pia

total path-integrated attenuation at Ku and Ka bands (4 byte float, nKuKa x nrayMS x nscan); from the 2BCMB Combined Algorithm (in MS).

correctedReflectFactor

attenuation-corrected radar reflectivity factor at Ku and Ka bands at 250 m sampling resolution (4 byte float, nKuKa x nbinC x nrayMS x nscan); from the 2BCMB Combined Algorithm (in MS).

multiScatMaxContrib

the maximum contribution by multiple scattering to a reflectivity simulation (4 byte float, nrayNS x nscan) in the given radar profile (in MS).

nubfPIAfactor

the fractional reduction of the Hitschfeld-Bordan estimated path-integrated attenuation for simulating the Surface Reference Technique path-integrated attenuation (4 byte float, nrayMS x nscan). Location (in NS).

Appendix B. Output Product Volumes

The volume of the Combined Algorithm output product, based upon the output parameters listed above, is approximately 150 MB per orbit file in internally compressed HDF5 format.

Appendix C. Processing Requirements

The current configuration of the Combined Algorithm requires input from six modules of the GPM Radar Algorithm: the Preparation Module, Vertical Profile Module, Classification Module, DSD Module, Surface Reference Technique Module, and the Environment Module. Output of these modules is expected from the Level 2 Radar Algorithm software; however, the computational requirements of this routine could add significant latency to Combined Algorithm processing.

A primary input to the Vertical Profile Module is JMA global analyses (GANAL) for standard processing and JMA global analyses/forecasts for near-real-time processing. Therefore, this input should be accommodated in PPS operations.

The current version of the algorithm requires approximately 15 minutes on a single PPS processing node to process a typical orbit of data, using multi-processor capability. Parallel processing will be achieved using POSIX thread libraries. Although some economies in the coding can reduce this processing time, they may result in degraded performance of the algorithm. Granules of DPR and GMI data will be subdivided into roughly 30 (300 DPR scan line) segments to keep required memory within limits on a given processing node.

Appendix D. Version Changes

V03 to V04 Changes

Many updates have been made to the Combined Algorithm Level 2 in the transition from V03 to V04, and the significant updates are summarized here. It may be noted at the outset, however, that the basic algorithm mechanics (i.e., estimation methodology) and output file structure have not changed. The estimation method filters ensembles of DPR Ku reflectivity-consistent precipitation profiles using the DPR Ka reflectivities, path integrated attenuations at Ku and Ka bands, and GMI radiances. The filtered profile ensembles are consistent with all of the observations and their uncertainties, and the mean of the filtered ensemble gives the best estimate of the precipitation profile.

In the Combined Algorithm V03 and V04, input data are passed from the Radar Algorithm Level 2 and Radiometer Algorithm Level 1C. However, to obtain better responsiveness of precipitation profile estimates to the GMI data in V04, input radiances are first resolution-enhanced to approximately the spatial resolution of the DPR resolution (~5 km). This enhancement is accomplished, at each channel frequency and polarization, using a statistically derived filter that predicts the DPR-resolution radiance from a weighted average of native-resolution GMI radiances in a small neighborhood of the observation to be enhanced. Filter weights are derived from regressions on synthetic radiance data, and the degree of enhancement is traded against noise amplification, with an optimal balance between enhancement and noise determined by cross-validation. Use of the resolution-enhanced data leads to a greater responsiveness of precipitation estimates to the GMI radiometer data, and a better fitting of those data. Moreover, data from all thirteen of the GMI channels are utilized in the V04 CMB algorithm, whereas data from only seven channels were used in the V03 algorithm.

In V03, the impact of multiple scattering on simulated reflectivities was crudely represented by typical reflectivity corrections (relative to single-scattering calculations) as functions of bulk scattering optical depth. This simple correction of reflectivities is replaced in V04 by the full simulation of multiple-scattering affected reflectivities using the 1D time-dependent radiative transfer model of Hogan and Battaglia (2008). This model is fully invoked only in situations where single- and multiple-scattering reflectivity simulations based

upon the ensemble-mean, Ku-consistent precipitation profile are significantly different, in which case the multiple-scattering model is applied to all ensemble member profiles to simulate the Ka reflectivities. The impact of multiple scattering on Ku reflectivities is generally much smaller than at Ka band and is not considered in V04.

The general parameterization of the effects of radar footprint non-uniform beamfilling by precipitation is the same in Combined Algorithm V03 to V04; however, the impact of non-uniform beamfilling on simulations of average path-integrated attenuation at the earth's surface is now properly represented in this parameterization in V04. This allows more consistent comparisons of simulated and surface reference technique (SRT) derived path-integrated attenuations in the algorithm.

Further, the use of individual SRT-based estimates of path-integrated attenuation at Ka band in V03 has been replaced by differential Ka-Ku path-integrated attenuation in the MS (Ku+Ka+GMI) mode of the Combined Algorithm V04. The precipitation-free differential Ka-Ku path-integrated attenuation reference is much more stable than the Ka-band reference, particularly over land surfaces, and this leads to less uncertainty in SRT-derived, differential Ka-Ku path-integrated attenuation estimates in precipitation regions. The SRT differential path-integrated attenuation is used to directly filter the precipitation profile ensembles, rather than inferring the individual Ku and Ka path-integrated attenuations from the differential path-integrated attenuation, and then filtering with those individual path-integrated attenuations.

The expected uncertainties of forward model simulations (relative to observations) prescribed in the ensemble filter kernel are changed from 1.4 dB to 3 dB for Ka-band reflectivities and from 5 ^{o}K to 6.1 ^{o}K for GMI radiances at frequencies above 37 GHz, going from V03 to V04. Expected uncertainties of path-integrated attenuations are maintained at 4 dB in the filter, and uncertainties of GMI radiances at frequencies up to 37 GHz are maintained at 5 ^{o}K.

V04 to V05 Changes

Numerous modifications have been made to the CMB Level 2 algorithm in the transition from V04 to V05, and the significant updates are summarized here. It may be noted at the outset, however, that the basic algorithm mechanics (i.e., estimation methodology) has not changed. The estimation method filters ensembles of DPR Ku reflectivity-consistent precipitation profiles using the DPR Ka reflectivities, path integrated attenuations and attenuated surface radar cross-sections at Ku and Ka bands, and GMI radiances. The filtered profile ensembles are consistent with all of the observations and their uncertainties, and the mean of the filtered ensemble gives the best estimate of the precipitation

profile. The output file structure is essentially the same as in CMB V04, but a few additional variables are included for diagnostic purposes.

In the CMB V03 and V04 algorithms, estimated precipitation profiles were constrained by estimates of total path-integrated attenuation from the satellite to the earth's surface, derived from the DPR algorithm's surface reference technique (SRT) module; Grecu et al. (2016). However, an alternative approach is to develop a model for the normalized radar cross-section (σ^0) of the surface at the Ku and Ka channel frequencies of the DPR and relate that to a model of the surface emissivities (ε) at the GMI frequencies. Such a σ^0/ε model was developed by Munchak et al. (2016). The model is used to effectively constrain the simulated surface σ^0/ε in the algorithm's simulations of attenuated surface cross-section and upwelling brightness temperatures, which are compared to the observed attenuated cross-sections and brightness temperatures. In the CMB V05 algorithm, both the path-integrated attenuations and attenuated surface cross-sections are utilized to constrain solutions, even though there is some redundancy between these two observables. It should be noted, however, that some redundancy in the information content of observations leads to greater suppression of uncorrelated noise in algorithm estimates.

Another new feature of the V05 algorithm involves the algorithm's simulation of path-integrated attenuation at Ka band. Using off-line, high-resolution simulations of attenuation based upon ground-based radar fields, it was determined that the Ka-band path-integrated attenuation in vertical columns over DPR-sized footprints, derived using a Hitschfeld-Bordan method as it is done in the CMB algorithm, is significantly overestimated in convective regions where the footprints are partially filled with precipitation. The degree of partial filling, however, can be estimated using a 3x3 array of DPR footprints centered on the footprint of interest. In the CMB V05 algorithm, a scaling parameter based on the 3x3 array is used to modify the Hitschfeld-Bordan derived path-integrated attenuation at Ka band to properly account for partial filling of the radar footprint by precipitation. At Ku band, the effects of partial footprint filling on path-integrated attenuation are much smaller and are neglected in CMB V05.

The CMB V04 algorithm estimates exhibited a lack of sensitivity to path-integrated attenuation, such that the scaling of estimated attenuation relative to reflectivity was sometimes inappropriately high (i.e., the scaling was adjusted little from the initial guess), leading to overestimation of rain rates. Two changes are introduced into the CMB V05 algorithm to obtain more appropriate sensitivity. First, the prescribed uncertainties of SRT-derived path-integrated attenuations are reduced, forcing greater fidelity of solutions to observed path-integrated attenuations. Second, a weak empirical constraint between particle size distribution mass-weighted mean diameters (D_m) and normalized intercepts (N_w) is imposed, such that larger D_m values tend to correlate with lower N_w

values. This constraint is implemented by making the normal first-guess of D_m but then using an empirical formula to calculate the corresponding N_w. The empirical N_w has the observed anti-correlated relationship with D_m (see Thompson et al. 2015), and it is used as an updated first guess for N_w. The algorithm then proceeds normally but with the updated first guess. This N_w-D_m constraint is important at low rain rates, where uncertainties in estimates of path-integrated attenuation estimated from the Level 2 radar algorithm (see Meneghini et al. 2000) make it impossible to adjust N_w (and the corresponding attenuation-reflectivity relationship) using path-integrated attenuation information. The two changes described here generally lead to lower rain rates using CMB V05.

Another aspect of the algorithm that is improved in V05 is the description of scattering by ice-phase precipitation particles. In all versions through V04, ice-phase precipitation particles were represented as spherically shaped, homogeneous mixtures of ice and air. In CMB V05, ice-phase precipitation in stratiform regions is represented using nonspherical particles with realistic geometries, as described in Kuo et al. (2016) and Olson et al. (2016). The rigorously computed microwave single-scattering properties of these particles are included in the algorithm's scattering tables. The nonspherical ice particles are less strongly forward scattering than spherical particles of the same mass, leading to substantially lower simulated upwelling microwave radiances at the higher-frequency GMI channels. The impact is to reduce CMB V05 algorithm-estimated snow water contents, since less snow is required to produce the same signal at the higher frequency channels. Mixed-phase particles are still described using spherical geometry models in V05.

The prescribed uncertainty of any observation in the CMB algorithm represents both the noise in the observation as well as the error in the simulation of that observation by the algorithm's forward model, and therefore it determines the degree to which the observation impacts estimates produced by the ensemble filter. As previously mentioned, the prescribed uncertainties of Ka-band reflectivities and Ku- and Ka-band path-integrated attenuations are modified in CMB V05. In addition, attenuated σ^0 observations are also introduced, and these observations are assigned uncertainties based on the variances of σ^0 for the given earth surface type, incidence angle, and wind conditions based upon a climatology of σ^0; see Munchak et al. (2016).

The prescribed uncertainties of Ka-band reflectivities are reduced from 3 dB in V04 to 2 dB in CMB V05. The uncertainty of Ku-band path-integrated attenuations is reduced from 4 dB to 3 dB. If path-integrated attenuation at Ka-band is available, the difference of the path-integrated attenuations (Ka – Ku) is used as an observable, with a prescribed uncertainty reduced from 4 dB to 2 dB in V05. This reduction of uncertainty is in recognition of the fact that the Ka-Ku path-integrated attenuation difference in non-precipitation situations provides a

more stable reference relative to that of either one of the two channels. Over open water surfaces, the uncertainties of the σ^0 at Ku and Ka band are set to their climatological variabilities, given the 10-m wind speed derived from reanalysis data. For other surfaces, the uncertainty of Ku σ^0 is also derived from its climatological variability, but it is limited to values above 2 dB, while the uncertainty of the Ka σ^0 is limited to values above 4 dB. Uncertainties in brightness temperatures are maintained at the V04 values of 5 K (at or below 37 GHz) and 6.1 K (above 37 GHz).

Grecu, M., W. S. Olson, S. J. Munchak, S. Ringerud, L. Liao, Z. S. Haddad, B. L. Kelley, and S. F. McLaughlin, 2016: The GPM Combined Algorithm. *J. Atmos. and Oceanic Tech.*, **33**, 2225-2245.

Hogan, R. J., and A. Battaglia, 2008: Fast lidar and radar multiple-scattering models. Part II: Wide-angle scattering using the time-dependent two-stream approximation. *J. Atmos. Sci.*, **65**, 3636–3651.

Kuo, K.-S., W. S. Olson, B. T. Johnson, M. Grecu, L. Tian, T. L. Clune, B. H. van Aartsen, A. J. Heymsfield, L. Liao, and R. Meneghini, 2016: The microwave radiative properties of falling snow derived from nonspherical ice particle models. Part I: An extensive database of simulated pristine crystals and aggregate particles, and their scattering properties. *J. Appl. Meteor. and Climatol.*, **55**, 691-708.

Meneghini, R., T. Iguchi, T. Kozu, L. Liao, Ken'Ichi Okamoto, J. A. Jones, and J. Kwiatkowski, 2000: Use of the Surface Reference Technique for path attenuation estimates from the TRMM Precipitation Radar. *J. Appl. Meteor.*, **39**, 2053-2070.

Munchak, S. J., R. Meneghini, M. Grecu, and W. S. Olson, 2016: A coupled emissivity and surface backscatter cross-section model for radar-radiometer retrieval of precipitation over water surfaces. *J. Atmos. Oceanic Technol.*, **33**, 215-229.

Olson, W. S., L. Tian, M. Grecu, K.-S. Kuo, B. T. Johnson, A. J. Heymsfield, A. Bansemer, G. M. Heymsfield, J. R. Wang, and R. Meneghini, 2016: The microwave radiative properties of falling snow derived from nonspherical ice particle models. Part II: Initial testing using radar, radiometer and in situ observations. *J. Appl. Meteor. Climatol.*, **55**, 709 – 722.

Thompson, E. J., S. A. Rutledge, B. Dolan, and M. Thurai, 2015: Drop size distributions and radar observations of convective and stratiform rain over the equatorial Indian and West Pacific Oceans. *J. Atmos. Sci.*, **72**, 4091-4125.